June 2019

Design and Testing of Experimental Langmuir Turbulence Facilities

Zongze Li
University of South Florida, 445721624@qq.com

Design and Testing of Experimental Langmuir Turbulence Facilities

by

Zongze Li

A thesis submitted in partial fulfillment
of the requirements for the degree of
Master of Science in Mechanical Engineering
Department of Mechanical Engineering
College of Engineering
University of South Florida

Major Professor: David Murphy, Ph.D.
Andres E. Tejada-Martinez, Ph.D.
Rasim Guldiken, Ph.D.

Date of Approval:
June 11, 2019

Keywords: ANSYS Simulation, Fluid Mechanics, PIV, Cylindrical Lens,
High Power LED

ACKNOWLEDGMENTS

First, I should sincerely thank to my professor, Dr. David Murphy, who gave me the chance to do this thesis and provided support, ideas and knowledge throughout the whole process. Without him, I might be still a layman of research. Just like Dr. Guldiken says: choosing a thesis will be much harder than taking 3 other courses. Sure it is, but I enjoyed it the whole time, which made me grow up in many areas.

I should also give my genuine thanks to Dr. Carlowen Smith, Dr. Michael Celestin and Kerry Battles. Carlowen worked closely with me, let me know how to deal with a hard thing step by step, how things work in a researching process and how to find potential problem in a design. Dr. Celestin and Kerry helped me make my design come true, gave me a lot of great improvements on the design and generously taught me knowledge in electronic engineering.

Finally, thanks again for all the people who helped me, without you, I could not have finished this paper so comprehensively.

TABLE OF CONTENTS

LIST OF TABLES

LIST OF FIGURES

ABSTRACT

Langmuir Circulation is a common phenomenon driven by wind in oceans and lakes and was first studied by Langmuir in 1927. According to various ocean observations, this kind of phenomenon plays an important role in many phenomena such as the aggregation of bubbles, the distribution of plankton as well as the mixing of spilled oil and sediment in the ocean. To study this, an experimental facility has been developed in the lab which creates a small scale version of Langmuir Circulation.

This thesis is about the design and testing of this tank and surrounding aluminum frame, as well as the design and construction of the illumination equipment (the Green Lantern 2.0) needed for Particle Image Velocimetry measurements within the tank. ANSYS will be used to show whether the tank is structurally strong enough to support the fluid. An enhancement is found that prevents a frontward bend of tank wall, which is analyzed by ANSYS to find an optimized construction to minimize tank deformation. Then, the Light-Emitting Diode (LED) and collimating lens selection for the Green Lantern 2.0 will also be shown in this paper. Besides, this thesis also presents preliminary flow measurement data acquired using the illumination equipment (the Green Lantern).

CHAPTER 1: INTRODUCTION

In lakes and the open sea, floating materials lying on the water surface aggregate into particular shapes, not in a random distribution. These materials tend to form many nearly parallel rows, some of which will also intersect with each other. This phenomenon is caused by Langmuir Circulation. This kind of circulation happens in the water column and is driven by the interaction of wind and waves, which affects the environment in the water.

The observation of Langmuir Circulation can be traced back to as early as 1773, Captain James Cook (1773), in the record of his first voyage, said: 'on the 9th of December 1768 we observed the sea to be covered with broad streaks of a yellowish colour, several of them a mile long, and three or four hundred yards wide.' Then Scoresby (1820), Darwin (1839), Dareste (1855), and Brown (1868) also observed this kind of phenomenon through seeing different color stripes in a particular pattern [1]. On August 7, 1927, Irving Langmuir noticed large quantities of seaweed arranged in particular shapes (e.g. long parallel rows); subsequently, during 1928 to 1929 he performed many experiments on this phenomenon on Lake George (near Bolton, New York). Finally he confirmed this phenomenon and published the paper 'Surface Motion of Water Induced by Wind' in 1938 [2]. This phenomenon was then named Langmuir Circulation and has subsequently been the subject of much study. Smith observed the growth of Langmuir Circulation and described this phenomenon in terms of its inducement, shape, and scale [3]. Thorpe did many observations, related wind speed to the appearance of sea surface and formulated Langmuir Circulation into sets of equations in his paper [4]. Weller and Price [5] used a current meter to measure the three components of velocity in order to look for evidence of Langmuir Circulation

within the mixed layer and characterize its strength as well as structure, and Weller et al [6] did find evidence of strong Langmuir cells. Then, with the help of Doppler sonar measurements, which has a range of up to 1400 m, Langmuir circulation also was detected in a study by Smith et al (1987) [7].

The formation of Langmuir circulation can be briefly described like this: wind blows across the sea surface, drags water in the wind direction, and creates shear force on the water surface. Stokes drift which is induced by the surface waves interacts with the shear caused by wind and finally generates Langmuir circulation. At the junction of two vortices, there will be two cases: one is that two vortices combine to make the water flow up (i.e. upwelling), the other is that they combine to make the water flow down (i.e. downwelling). For the second case, if particles in the water (e.g. sargassum, oil droplets) are buoyant and can overcome the downward force caused by the fluid, then they will accumulate in the center of the two vortices in long windrows [8]. The axis of the cells of Langmuir circulation has an angle of up to 20° to the right of the direction of the wind [9] and the distance between cells can vary from 1 m to 300 m.

Langmuir Circulation plays many roles in the sea or lake systems. For example, the patchy distribution of phytoplankton induced by Langmuir Circulation will consequently affect the distribution of organisms that feed on phytoplankton [8]. In addition, many researchers have found that Langmuir Circulation can reach throughout the mixed layer and even to the bottom of the water column; it is thus able to entrain materials from the sea floor and mix them up into the water column. Driven by a strong storm, the vertical extent of the cells becomes more severe [10-11]. Further, Chiba and Baschek found that Langmuir Circulation can enhance the speed of various kinds of gas exchange happening on the water surface [12]. Hammer and Schneider also discovered that Langmuir circulation plays an important role in the relation of prey, predators, and

competitors in the Bering Sea by increasing or decreasing the spatial aggregation of medusa [13]. Barstow reviewed the Langmuir Circulation literature and concluded in his review paper that Langmuir circulation not only plays an important role in the flow of the ocean, but also is important to marine biologists, chemists, and even geologists [14].

As researchers have studied Langmuir Circulation, its importance has become more and more evident. Because of the difficulty of studying Langmuir Circulation in the field, we have designed and built an experimental facility that creates a two dimensional "cartoon" of Langmuir Circulation in an acrylic tank in the laboratory. The focus of this thesis is on the design, testing, and subsequent modification of this experimental facility for future experiments examining the interaction of buoyant oil droplets and heavy sediment particles in Langmuir Circulation.

CHAPTER 2: TANK SIMULATION

2.1 Introduction

As previous chapter mentioned, Langmuir Circulation consists of pairs of counter-rotating vortices, the experimental facilities (shown in Figure 2.1), which are used to simulate one of this pair of flow, consist of an acrylic tank (the object of the simulation in this chapter, shown in Figure 2.2), motors, and conveyor belts. The water in the tank is driven by the conveyor belts on both sides of the tank to create a pair of counter-rotating vortices. Then, a high speed camera is used to capture the flow in front of the tank.

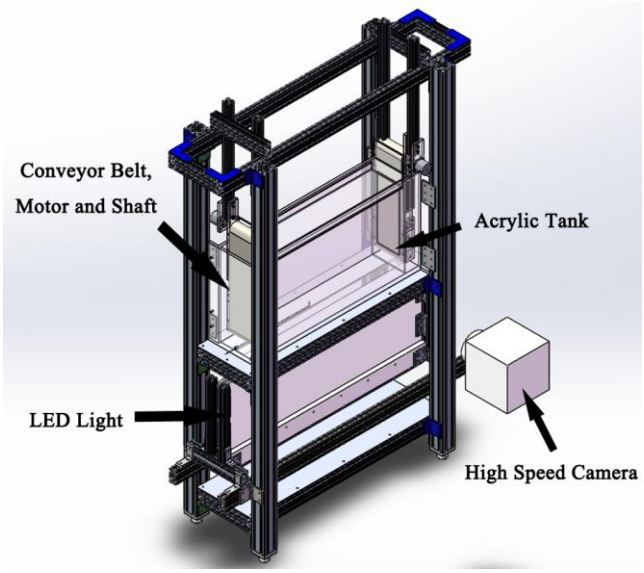

Figure 2.1 CAD Drawing of Langmuir Circulation Experimental Facility

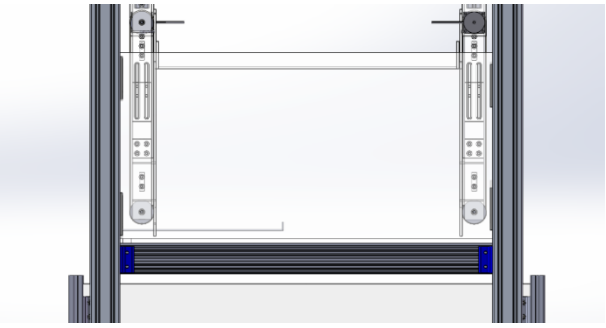

Figure 2.2 Front View of Langmuir Circulation Experimental Facility

However, it is observed that, when filled with water, the tank walls deform (up to 2 cm as will be shown in the following paragraphs). This may cause two problems: one is that the tank wall could break because of either the large deformation or the fatigue failure caused by multiple cycles of filling and draining it. The other concern is that since the high speed camera captures images through the tank wall, the wall deformation could distort the images.

Hence, in this chapter, ANSYS software will be used to show the performance of the acrylic tank. By using the Static Structural module, this software will determine how the tank will be in the real world from the aspects of deformation, equivalent stress and safety factor when the tank is 25%, 50%, 75%, and full of water. Then another simulation in which a brace is added across the opening of the tank is done to show the structural stability and reduction in deformation of the tank.

2.2 Model Geometry

Two simulation models are tested: one is the tank alone, the other is the tank held with an aluminum clamp on the top in order to decrease the tank wall deformation. The original tank is modeled as a rectangular box, of which the length is 100 cm, the height is 50 cm, the width is 20 cm, and the wall thickness is 1.2 cm. In order to set the amount of water within the tank, the tank is divided vertically into 4 parts by 3 enclosed lines. The vertical distance between those enclosed lines is 12.5 cm. The configurations and the final model are shown in Figure 2.3 and Table 2.1.

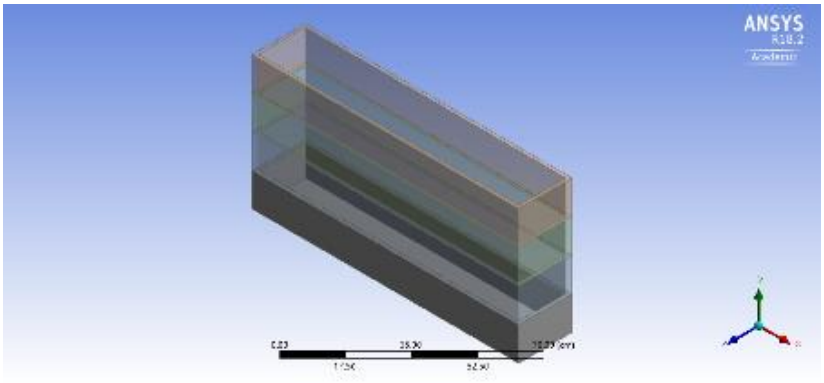

Figure 2.3 Original Tank Model

Table 2.1 Parameters of Original Tank

Property	Value (cm)
Tank Length	100
Tank Width	20
Tank Height	50
Tank Wall Thickness	1.2

Since initial experiments showed a large amount of tank wall deformation when the tank was filled, the need for a brace or clamp at the tank surface was apparent. Three different aluminum brace designs were generated and tested in ANSYS. Each brace consisted of a pair of extruded aluminum rails (80/20 Inc.) laying along the top of the tank walls. These rails are joined across the tank by a pair of short extruded aluminum rails (80/20 Inc.) positioned at different distances from each other. The position for these rails which minimizes deformation and stress is found in this paper by changing the short beam location. Finally, the three models and the distance between the two short beams are shown in Figures 2.3, Figure 2.4, Figure 2.5, and Table 2.2.

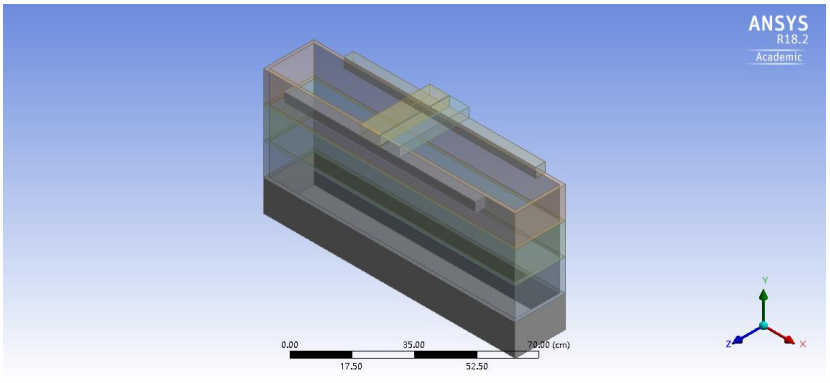

Figure 2.4 Improved Tank Clamp at Center

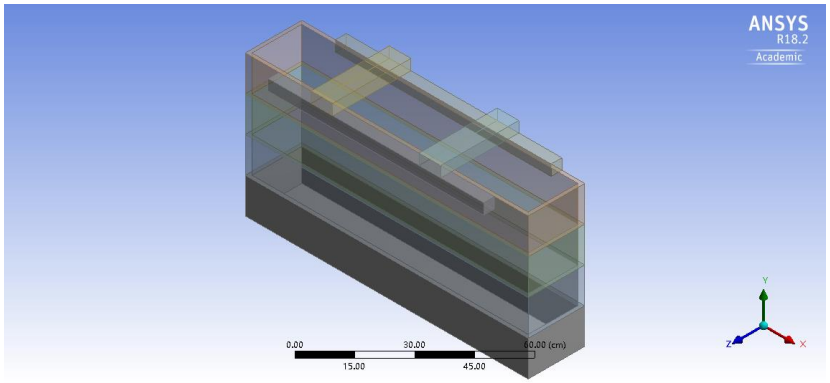

Figure 2.5 Improved Tank Clamp at Half of Long Beam

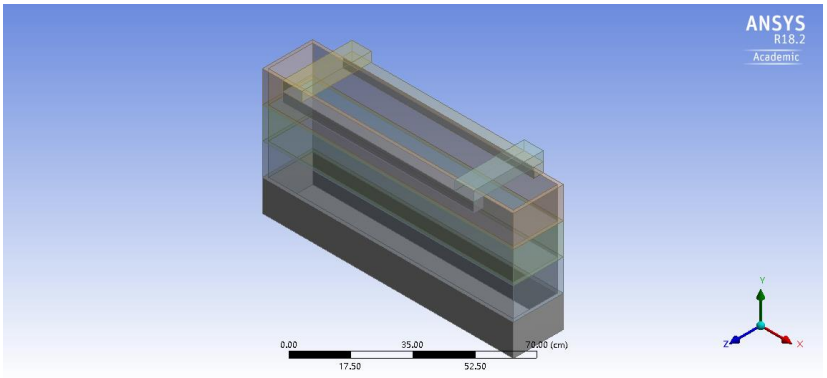

Figure 2.6 Improved Tank Clamp at End of Long Beam

Table 2.2 Distance between Two Short Beams

Location of Short Beams	Distance Between Center of Short Beams (cm)
At the center of long beam	8.00
At the half of long beam	38.10
At the end of long beam	68.58

2.3 Boundary Conditions

After creating the models in ANSYS, the next step is to set the boundary conditions. For the Static Structural module, the boundary conditions are fixed support, pressure, force, and material property. First, the acrylic material properties are needed since ANSYS doesn't have this information in its engineering source. The material properties are set as in Table 2.3 and Table 2.4.

Table 2.3 Aluminum Physical Properties

Property	Value
Density	2770 kg/m^3
Young's Modulus	71000 MPa
Poisson's Ratio	0.33
Bulk Modulus	69608 MPa
Shear Modulus	26692 MPa
Tensile and Compressive Yield Strength	280 MPa

Table 2.4 Acrylic Sheet Physical Properties

Property	Value
Density	1180 kg/m^3
Young's Modulus	2760 MPa
Poisson's Ratio	0.37
Bulk Modulus	3538.5 MPa
Shear Modulus	1007.3 MPa
Tensile Yield Strength	64.8 MPa
Compressive Yield Strength	110 MPa

2.3.1 Original Tank Boundary Conditions

For Static Structural boundary conditions, the material is set as an acrylic sheet first. There is only one part, so no connections need to be set. For mesh statistics, coarse quality is chosen, resulting in 24821 nodes and 4589 elements, as Figure 2.7 shows. For the fixed support option, the outer bottom of tank is chosen; hydrostatic pressure is used to simulate the real water pressure. Figure 2.8 shows the geometry of this case, the inner side faces of the tank are selected to set the hydrostatic pressure. Fluid density is selected to match the seawater in the Gulf of Mexico (e.g. 1027 kg/m^3)

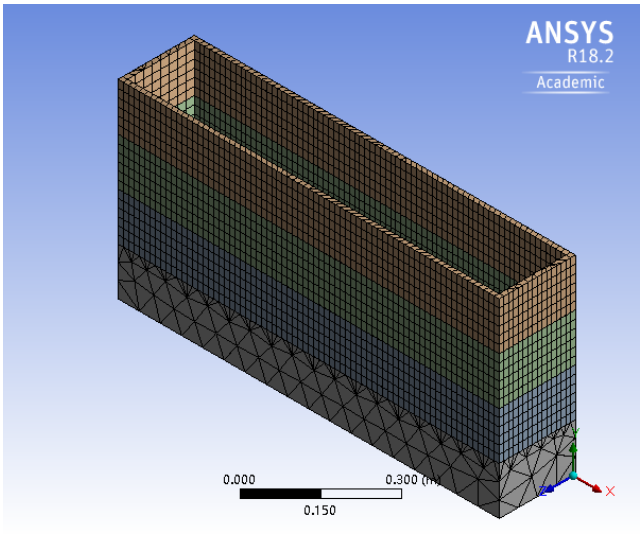

Figure 2.7 Original Tank Mesh

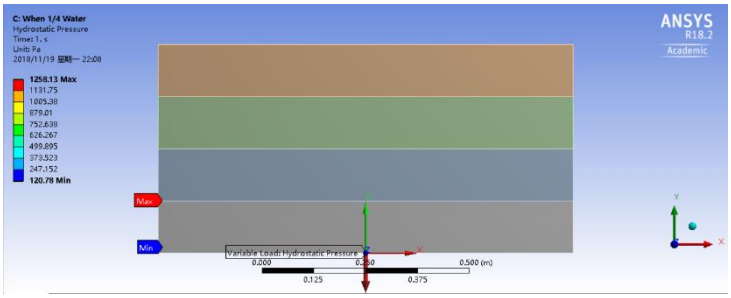

Figure 2.8 Hydrostatic Pressure for 1/4 Water

2.3.2 Boundary Conditions for the Improved Tank

Four aluminum beams are added on the top of the tank, so the material is set to aluminum alloy for the beams. There are two parts, the tank and the brace, so a connection set is needed, as shown in Figure 2.9. The connection type is set to rough, so that there is friction between tank and clamp. A coarse mesh is used in this setting (there are 27665 nodes and 5005 elements), and the mesh is shown in Figure 2.10. The static structural settings are similar to the original tank case. The water is full in this case.

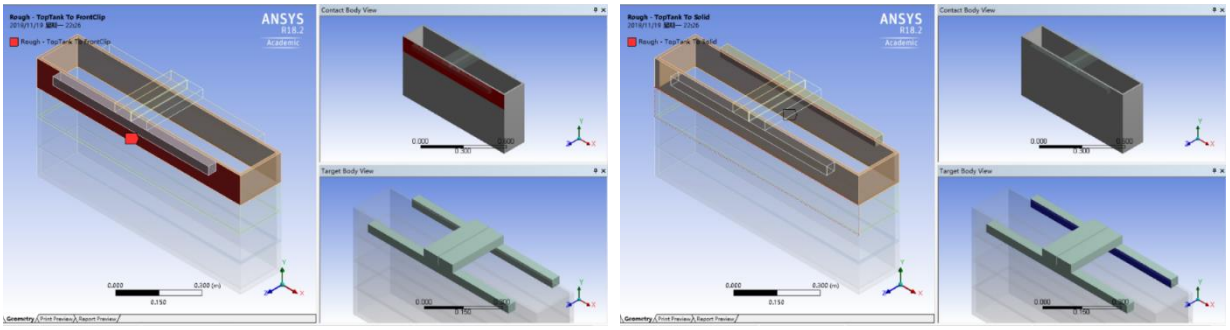

(a) (b)

Figure 2.9 Connection Setting. (a. connection between front long beam and front wall of tank; b. connection between back long beam and back wall of tank)

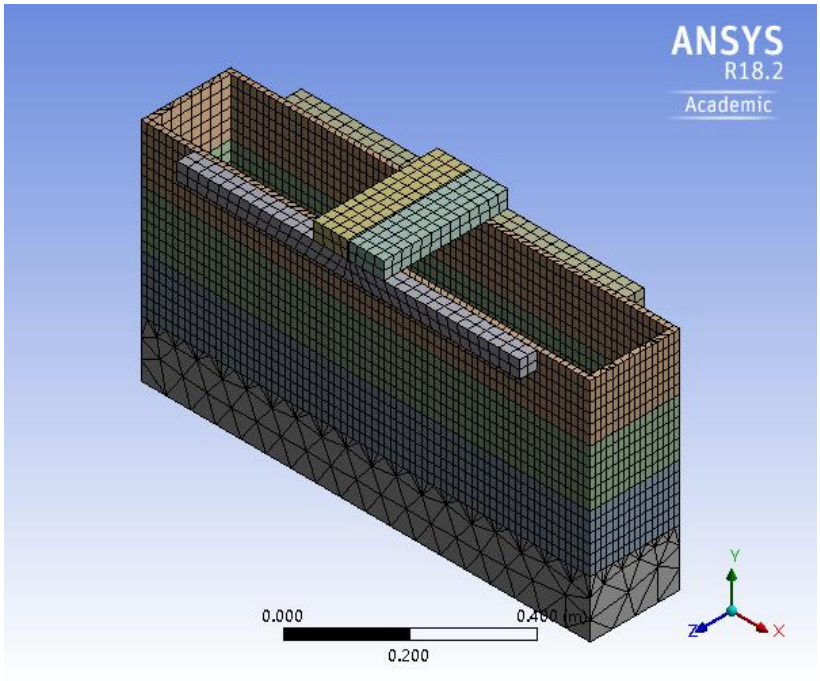

Figure 2.10 Improved Tank Mesh

2.4 Mathematic Methods

The whole process of doing a simulation can be divided into the following steps:

(1) Physical System

(2) Mathematic Model

(3) Finite Element Method (FEM) Model

(4) Local Elemental Equation

(5) Global Equation

(6) Apply Boundary Condition

(7) Solve for Unknowns

Step (1) is the description of the model in real world, including analysis of its dimensions, materials, and forces. Step (2) is to choose a proper mathematic model; when using the software, the mathematic model will be selected automatically. For example, when analyzing the deformation, Hooke's law will be selected for this kind of simulation. However, the safety factor criteria is selected manually. These differ according to whether the material is brittle or ductile. In this case, aluminum is ductile material, and the criterion for ductile material is the Max Equivalent Stress Theory. However, acrylic is a kind of brittle material, which uses Mohr-Coulomb Theory as a criterion.

Step (3), step (4) and step (5) are the pre-processing steps for ANSYS. The mesh will be generated in step (3), and steps (4) and (5) are a series of formula transformations calculated by computer. In those formulas, there are several unknown. Some unknowns need to be specified in step (6), which sets the boundary conditions, and the other unknowns are the results, such as total deformation, equivalent stress, and safety factor. After setting all needed boundary conditions, the software will give a comprehensive result for every element (this is generated in step (3)).

For the result, in this paper, total deformation, equivalent stress and safety factor will be analyzed. Total deformation determines the distance the element moves in the 3-D space, equivalent stress (also called von Mises stress) shows the 3-D stress state at every element, and safety factor is used to judge the stability of every element.

2.5 Simulation Results

In this section, the results of the tank with and without the improvement will be shown in terms of their total deformation, equivalent stress and safety factor. Some figures which show the total deformation, equivalent stress, and safety factor vs the amount of water in the tank will be made to show the trend while the amount of water in the tank is changed.

2.5.1 Original Tank Results

Figure A.1, Figure A.2, Figure A.3 (in Appendix A) and Figure 2.11 are the maximum deformation, stress, and safety factor results for four situations in which the tank is 1/4, 1/2, 3/4 and completely full of simulated seawater, respectively. For the total deformation, the distributions are similar, which the maximum point happens at the center of the top edge of the tank while the minimum point happens at the bottom of the tank. As expected, the maximum deformation occurs in the middle of the long wall and ranges in value from $7.49*10^{-5}$ m to $1.99*10^{-2}$ m. The field of equivalent stress changes a lot as the amount of water increases. When the water is less than 3/4 of the tank, the maximum equivalent stress happens on the front and back walls, and the maximum point happens on the side walls of the tank when the tank is completely filled with water. This may be caused by that the deformation becomes larger as the amount of water increases. At first, the side walls only burden the hydrostatic pressure. As the deformation become larger, the side walls also burden the internal stress from the deformation. Hence, the maximum equivalent stress finally happens on the side walls.

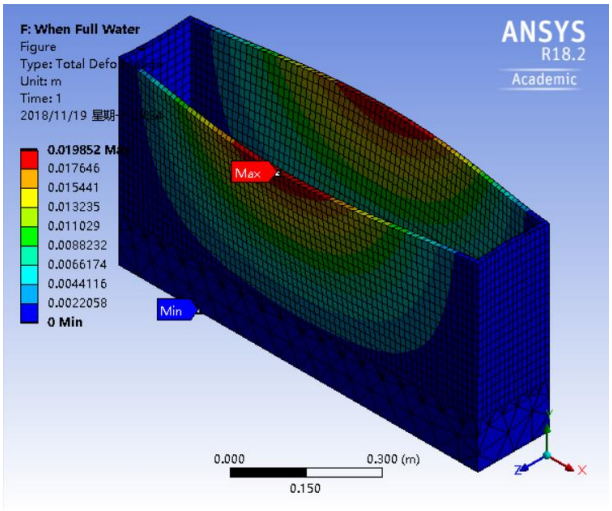

(a)

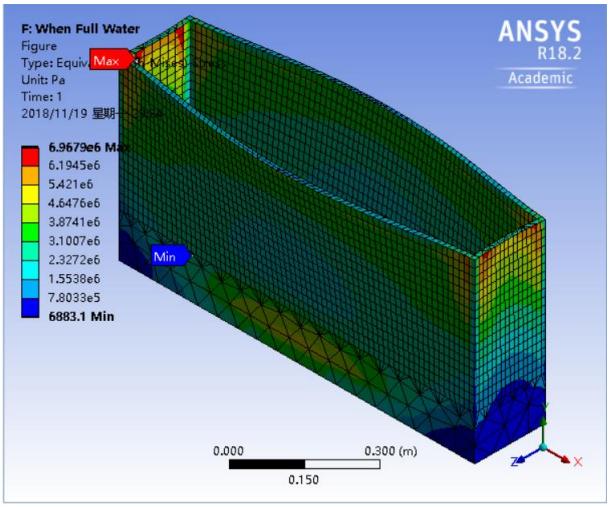

(b)

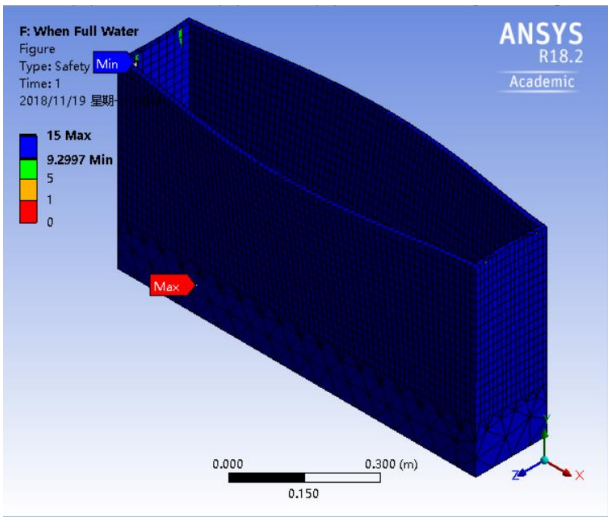

(c)

Figure 2.11 Full Water Tank Results. (a. Total Deformation, b. Equivalent Stress, c. Safety Factor)

Maximum values for the deformation, stress, and safety factor are extracted from ANSYS and presented in Table 2.5 and Figures 2.12 and Figure 2.13. From these figures and table, it can be seen that total deformation and equivalent stress increase slowly when the water is less than 5/8 (the point between 1/2 and 3/4). After that, the slope becomes sharper.

Table 2.5 Results of Tank Simulation

Water Status	Total Deformation (m)		Equivalent Stress (Pa)		Safety Factor	
	Max	Min	Max	Min	Max	Min
1/4	$7.49*10^{-5}$	0	$7.98*10^{4}$	63.37	15	15
1/2	$1.30*10^{-3}$	0	$7.49*10^{5}$	$1.12*10^{3}$	15	15
3/4	$6.50*10^{-3}$	0	$2.34*10^{6}$	$2.87*10^{3}$	15	15
1	$1.99*10^{-2}$	0	$6.97*10^{6}$	$6.88*10^{3}$	15	9.3

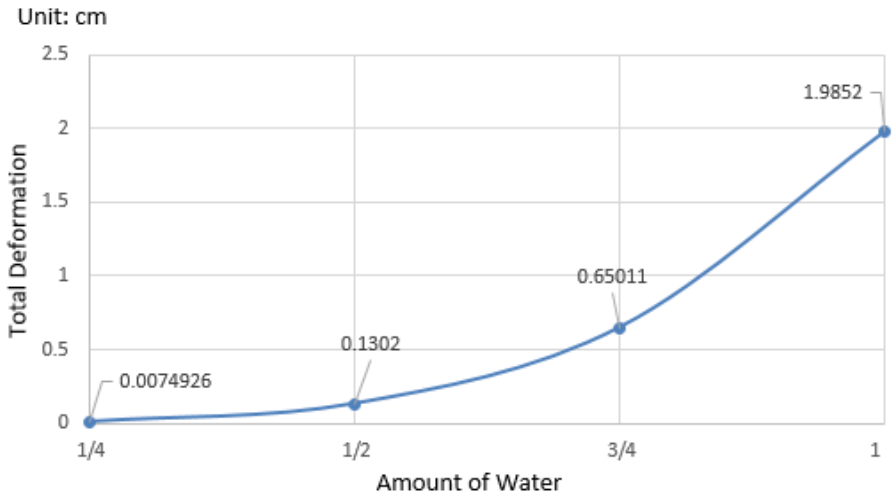

Figure 2.12 Total Deformation of Original Tank

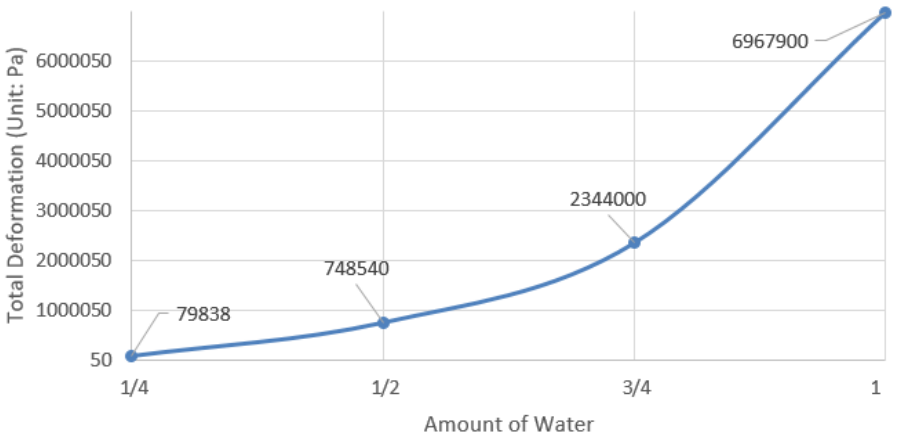

Figure 2.13 Equivalent Stress of Original Tank

Finally, the results show that, in terms of static structural stability, the tank can safely be filled with water. However, the experiment requires capturing the velocity field inside the tank and the deformation will cause a curvature at the front surface of tank which will distort images recorded through this surface. Therefore, it is necessary to find a solution for this issue.

2.5.2 Improved Tank Results

To eliminate the curvature at the front surface of tank, a clamp-shape construction is used to hold the top of tank. Full water is set in this simulation and the position of clamp is changed to find the best position for the top beams. Figure A.4, Figure A.5 (in Appendix A) and Figure 2.14 show the results and the maximum and minimum value for each simulation and the results are organized in Figure 2.15, Figure 2.16, Figure 2.17 and Table 2.6.

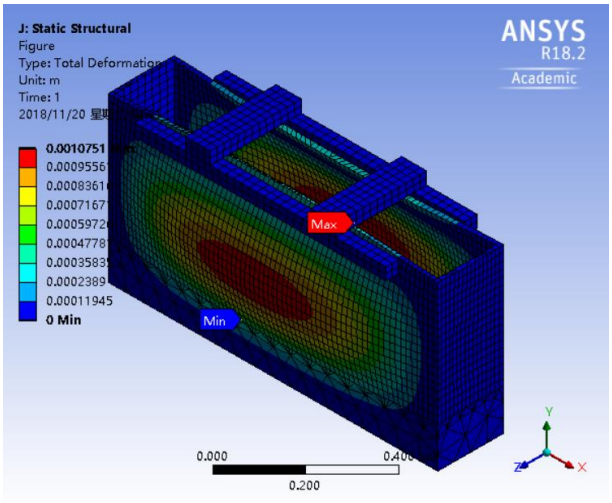

(a)

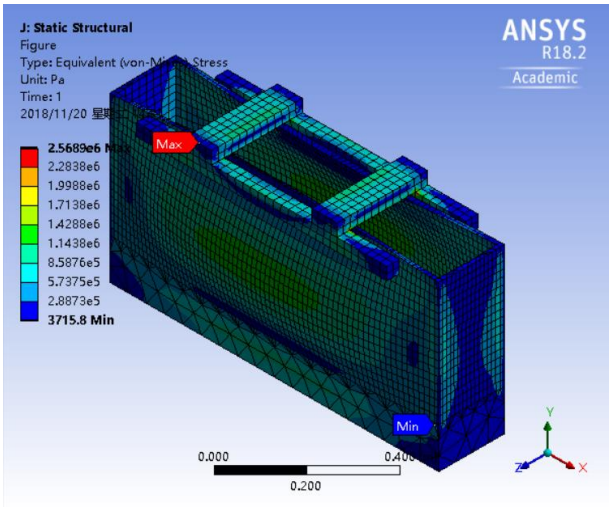

(b)

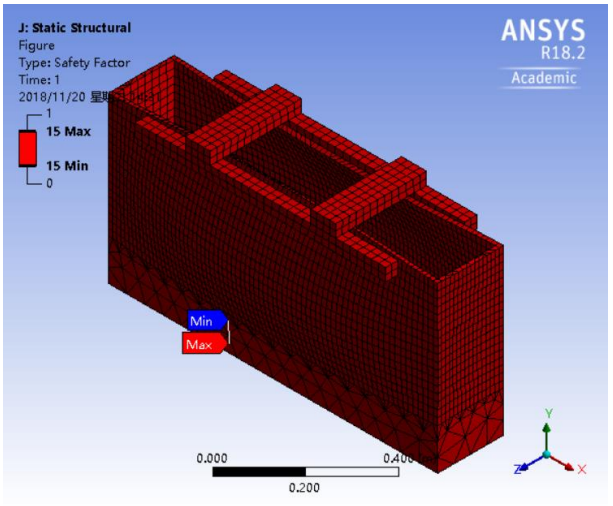

(c)

Figure 2.14 Report of Improved Tank When Clamp Is at Half of Long Beams. (a. Total Deformation, b. Equivalent Stress, c. Safety Factor)

Table 2.6 Results of Improved Tank Simulation

Beam Position	Total Deformation (m)		Equivalent Stress (Pa)		Safety Factor	
	Max	Min	Max	Min	Max	Min
Center	$1.0754*10^{-3}$	0	$6.47*10^{6}$	$3.54*10^{3}$	15	15
Half	$1.0751*10^{-3}$	0	$2.57*10^{6}$	$3.72*10^{3}$	15	15
End	$1.09*10^{-3}$	0	$4.15*10^{6}$	$3.64*10^{3}$	15	15

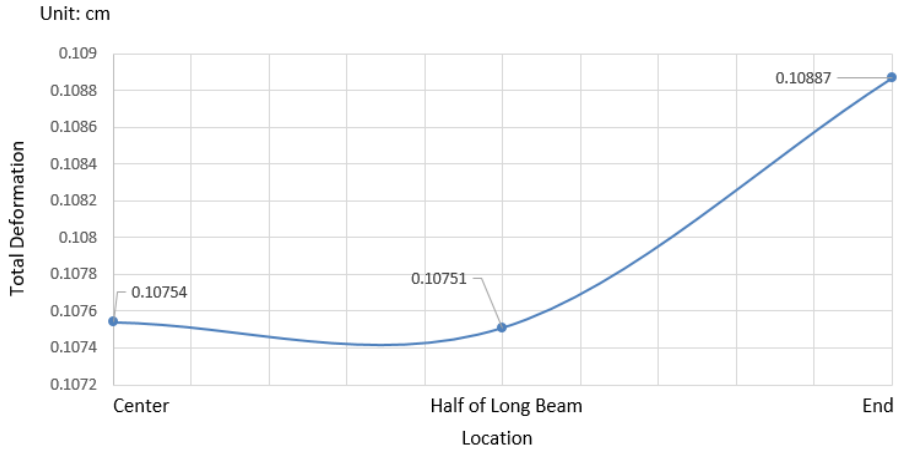

Figure 2.15 Max Total Deformation of Improved Tank

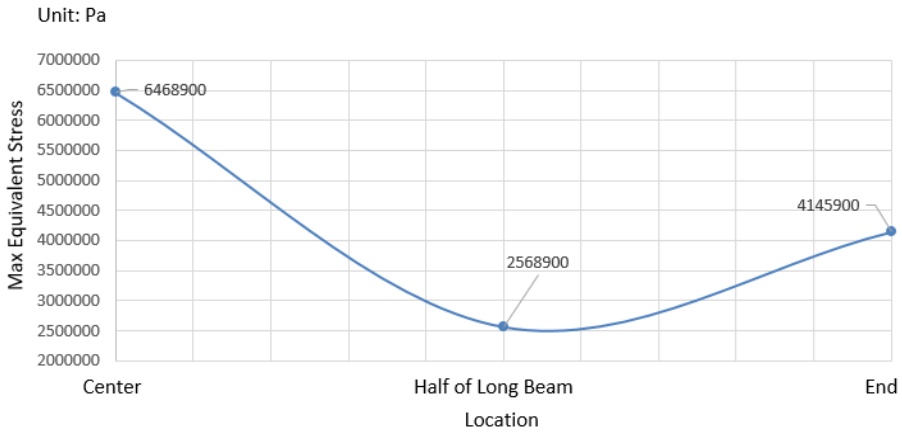

Figure 2.16 Max Equivalent Stress of Improved Tank

It can be found that maximum equivalent stress happens when the distance between the two beams is 0.55 of the length of horizontal beam. The minimum value of maximum total deformation happens when this distance is 0.35. However, the maximum total deformation is ignored because of its scale, the maximum total deformation is 1.0887 mm and it is small enough to ignore compared with the dimension of tank. The optimized position is therefore around 0.55.

2.6 Comparison of Distortions between Original and Improved Tanks

Figure 2.17 Image of Water-Filled Tank without Clamp

Figure 2.18 Image of Water-Filled Tank with Clamp

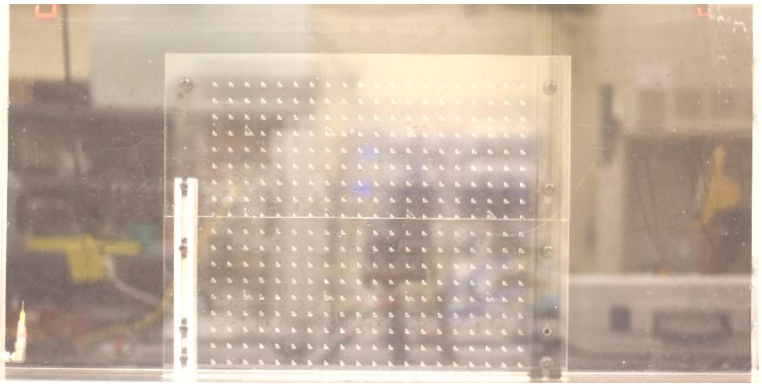

Figure 2.19 Image of Tank without Water

Images showing the optical distortion of the tank with and without the clamp are shown in Figures 2.17 and Figure 2.18. Figure 2.19 shows a similar image for the empty tank (as a reference image). From the reduced distortion of the image background, it is obvious that the deformation of the front surface of the tank is reduced by the clamp on the top of the tank, which means the distortion is reduced when capturing images by high speed camera.

2.7 Conclusion

Generally, when the water in tank is less than 1/2, it is not necessary to add a clamp on the top of tank; for that the deformation is small enough to ignore compared with the dimension of tank. When the water is more than 1/2, a clamp which can hold the tank on the top needs to be added in order to keep the front surface as least deformed as possible.

For the clamp added on the top of the tank, the optimized distance between the two short beams is 0.55 times of the length of the long beam. This distance can distribute the force field most evenly and get the smallest maximum equivalent stress.

CHAPTER 3: ILLUMINATION (GREEN LANTERN 2.0) FOR EXPERIMENT

3.1 Motivation

Currently, a plane of illumination in this center plane is provided by the Green Lantern (to be described below), and this plane of light enters the bottom of tank through a slot at the bottom of the tank, shown in Figure 3.1. Using flow tracers of 500 micron – 1.00 mm Pliolite-AC80, images of the flow are captured by a Phantom VEO 640S Digital High Speed Camera, which has the resolution of 2560 pixels × 1600 pixels. Finally, Particle Image Velocimetry (PIV) is used to analyze the images received from the camera to calculate velocity fields in the Langmuir Circulation facility.

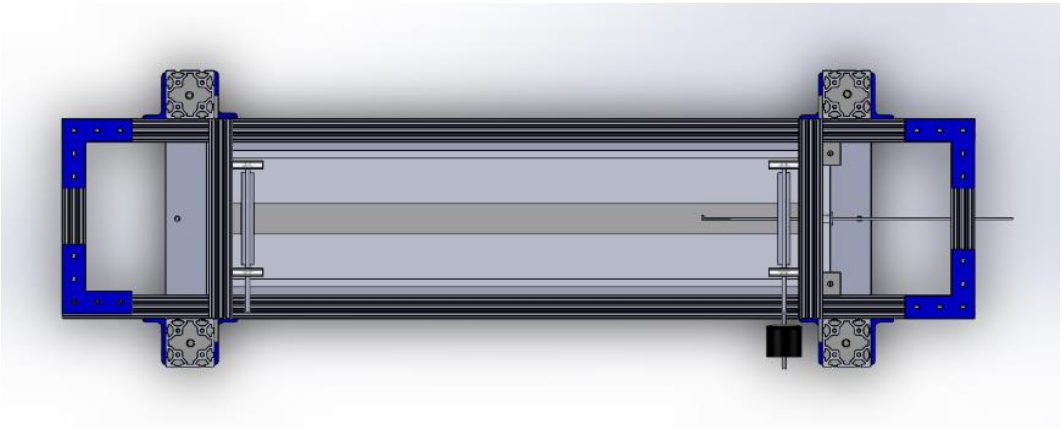

Figure 3.1 Tank Top View

However, the Green Lantern, which was provided by Dr. Sarah Delevan, provides insufficient illumination as well as insufficient length (the tank is 100 cm long but the Green Lantern is only 74.3 cm long). Hence, brighter and longer illumination equipment is needed. Thanks to the recent

evolution of Light Emitting Diode (LED) technology, a 10 mm^2 LED can provide 163 lm (Lumen is a unit to quantify the total amount of light an object emits per unit time) while the current Green Lantern uses an LED which only produces 51.7 lm on a 7 mm × 9 mm surface area. Recently, other researchers have investigated and taken advantage of LEDs as a light source for fluid dynamics experiments. For example, Buchmann and Willert et al investigated the feasibility of high-power LED illumination for tomographic particle image velocimetry (PIV); in their paper, they use a custom –built driver to power a Luminus PT-120 high-power LED at pulsed currents up to 150 A in the time duration of 1μs [15]. Estevadeordal and Goss used LEDs in an inverse way called Particle Shadow Velocimetry which used LEDs to illuminate a 2-D surface behind the object field in the air and made tracers in a shadow instead of directly lighting them up [16]. Broeder and Sommerfeld also used LEDs to illuminate a 2-D surface as a background light source in addition to a laser in order to solve the void scattering on the surface of the bubbles caused by the strong absorption of the laser light sheet [17]. Finally, Mirek and Tomasz et al did a comprehensive comparison of Laser Diodes (LD) and Light-Emitting Diodes (LED) in terms of their history, evolution principles, and advantages as well as shortcomings in the area of analytical chemistry [18].

The aim of this thesis chapter is therefore to design and build a new illumination facility (the Green Lantern 2.0) which will take advantage of the recent advances in LED technology. Further, the Green Lantern 2.0 aims to provide a light sheet with adjustable thickness, a capability not found in the original Green Lantern. The Green Lantern 2.0 is 120 cm which is 20 cm longer than the tank in order to provide uniform brightness of the light sheet along its length.

3.2 Principle

The design of the Green Lantern 2.0 is based on that of the original Green Lantern provided by Dr. Sarah Delavan. In the original Green Lantern, 33 LEDs with their own collimated lenses are arranged in 3 modules (11 LEDs on each module) and the useless light is covered by a pair of baffles (e.g. large flat parallel sheets), shown in Figure 3.2. The light comes out from the light source and is collimated by the collimating lens. Finally the pair of baffles cover the useless light to form a light sheet.

Figure 3.2 Two Green Lanterns. (The longer one is the Green Lantern 2.0; the shorter one is the original Green Lantern)

The design in this paper uses similar means to achieve a 2-D light sheet: LEDs are placed in a line as in Figure 3.3 and the unneeded light is blocked as in Figure 3.4. The baffle sheets are adjustable in order to change the thickness of light.

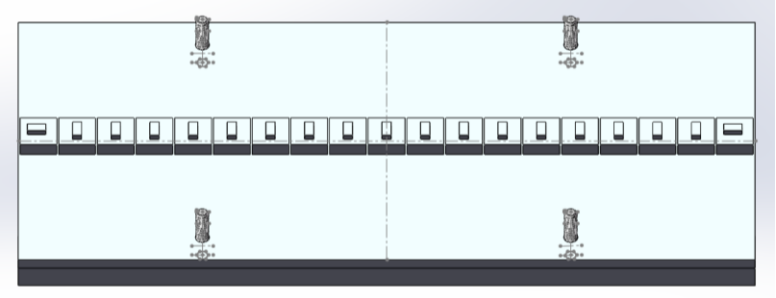

Figure 3.3 LED Arrangement in One Module

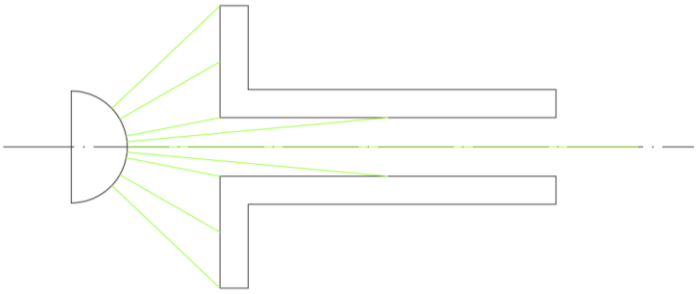

Figure 3.4 Use Baffle to Block Light

In addition, the usage of light is low if there is no collimator between the baffle and the LED, in which case only the light which is parallel to baffle can access the slot. So, in order to increase the usage of light, collimator lenses are used in front of the LEDs. Then, there are three ways to position the light source relative to the lenses: inside the focus point, at the focus point and outside the focus point. Different locations will cause different light paths: when the LED is placed inside the focus point, the light paths are diverging when exiting the lens; when at the focus point, the light paths will be parallel; and when outside the focus point, the paths will go to a point then diverge again. Figure 3.5, Figure 3.6 and Figure 3.7 show these three cases. Both positions inside and outside the focus point will finally get a lower usage of light because the baffles will eventually block the non-parallel path. So, it is essential that the light source is put at the focus point.

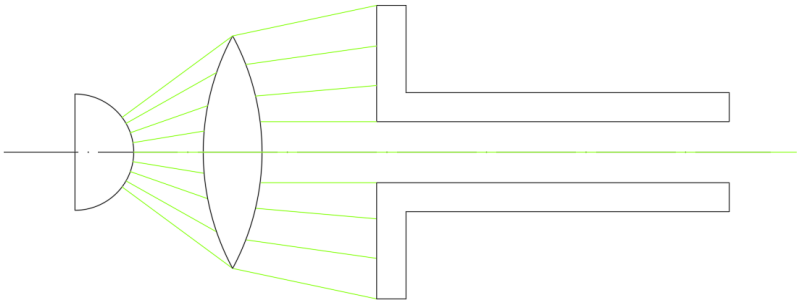

Figure 3.5 LED Puts inside Focus Point

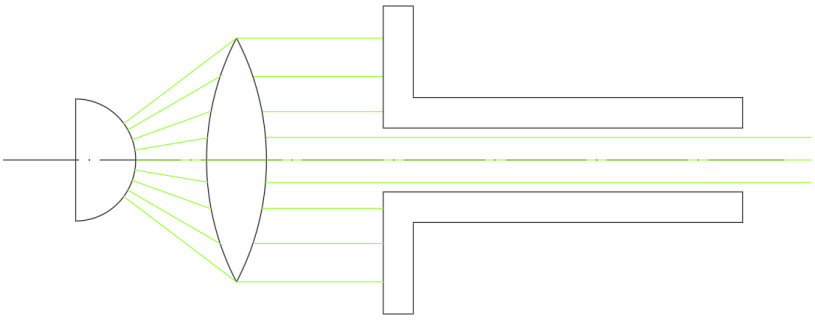

Figure 3.6 LED Puts at Focus Point

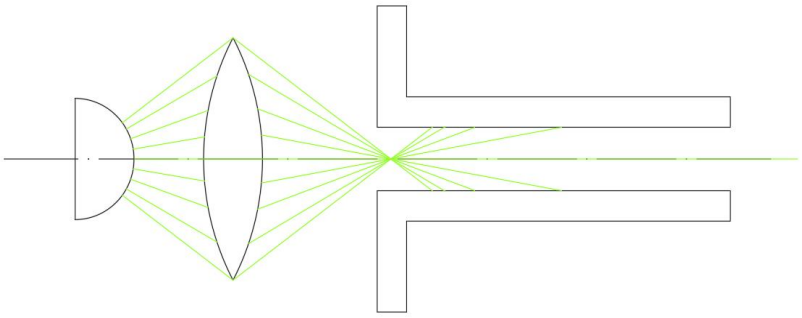

Figure 3.7 LED Puts outside Focus Point

3.3 Experiment of LED Box for Green Lantern 2.0

In this section, the process of how to choose the proper collimator lens and light source is explained. The process is mainly divided into three sections: LED selection, cylindrical lens selection, and using different sizes of a certain kind of cylindrical lens.

3.3.1 LED Selection

In preliminary testing, I used two kinds of LEDs. The first one has only one emitter on the base (Rebel 10mm Square LED) while the other has 4 emitters close to each other on the base (Luxeon Z LED), as shown in Figure 3.8. Only a single LED (not a line of LEDs) is used in all the following experiments. In these tests, the LED was positioned 1 m away from white paper upon which the LED light beam shines.

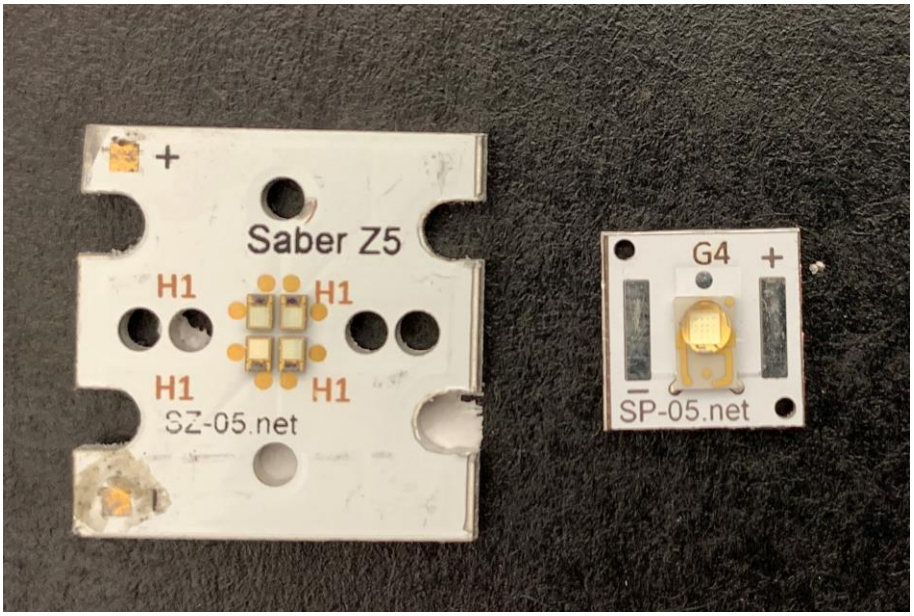

Figure 3.8 Two Kinds of LEDs Used in Experiments. (Left is Luxeon, Right is Rebel)

(1) Rebel 10 mm Square LED and Rod Lens

The LED and lens are shown in Figure 3.9, the center of LED, the axis of the rod lens (2.54 cm diameter) and the center of the white paper are set in a horizontal line. Because we use the rod lens, the image projected on the other side will be stretched to a line. The brightness is highest at the middle and gradually decreases away from the middle, shown in Figure 3.10.

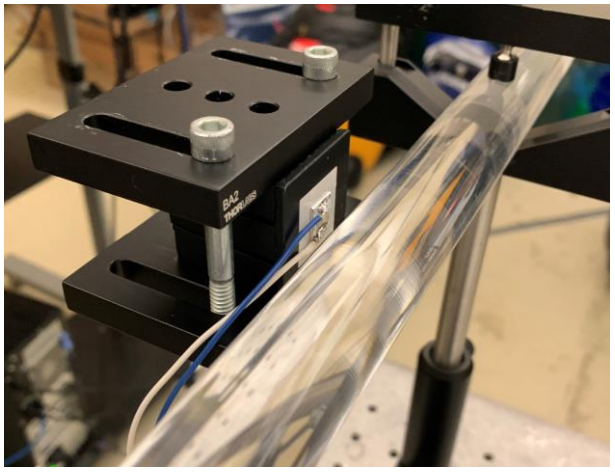

Figure 3.9 Rebel LED and Rod Lens Experiment Configuration

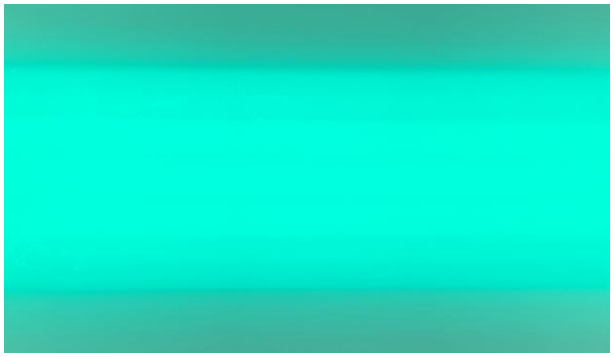

Figure 3.10 Image of Rebel and Rod Lens

(2) Luxeon Z LED and Rod Lens

The experimental configuration is shown in Figure 3.11. The LED has 4 emitters on the base, which is 2 rows of 2 in each row. This causes the image to have two lines, shown in Figure 3.12, which is not ideal. The projected gap will be dramatically large even when the original one is very small. The Luxeon LEDs were thus not used in the following experiments.

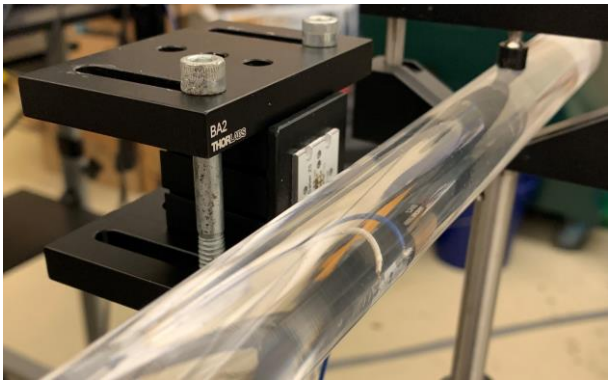

Figure 3.11 Luxeon and Rod Lens Experiment Configuration

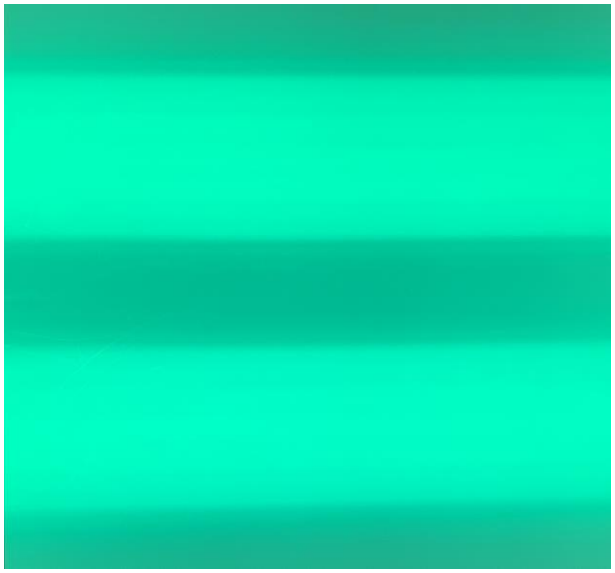

Figure 3.12 Image of Luxeon and Rod Lens

3.3.2 Using Different Cylindrical Lenses

For the selection of lenses, two kinds are considered; one is an acrylic rod lens and the other is Fresnel cylindrical lens, shown in Figure 3.13. From what we have, the images of these two kinds of lenses are nearly the same, but the Fresnel lens has advantage in its shape: it is easy to fix and occupies less room. Furthermore, the brightness of the image from the Fresnel lens is slightly brighter than the other one, as shown in Figure 3.14 and Figure 3.15. For these reasons, the Fresnel lens is selected for the collimating lens.

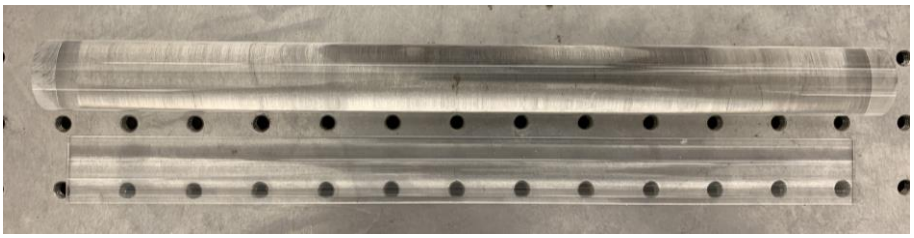

Figure 3.13 Two Kinds of Lenses. (The top is a rod lens; the bottom is a Fresnel lens)

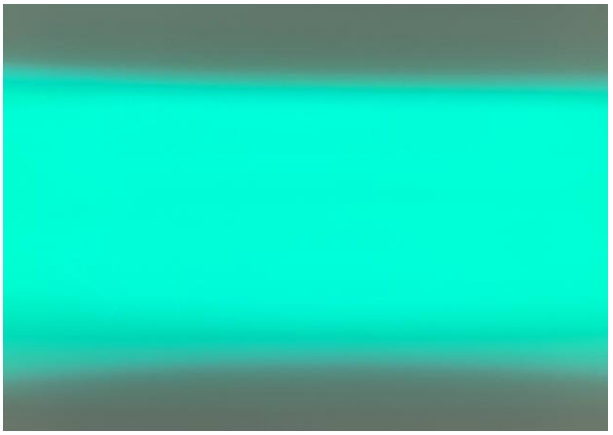

Figure 3.14 Image of Fresnel Lens

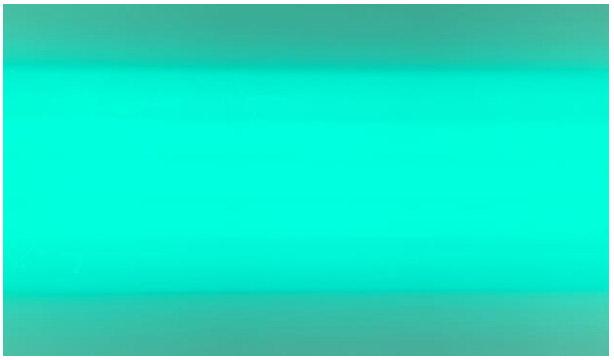

Figure 3.15 Image of Rod Lens

3.3.3 Using Different Sizes of Fresnel Lenses

After choosing the type of LEDs and lenses, there is another question: the size of lens. To solve this question, three lenses with different focal lengths are chosen to see what focal length is proper for our project, the three different focal lengths are 0.64 cm (1.27 cm wide), 1.91 cm (2.54 cm wide), and 5.08 cm (5.72 cm wide), shown in Figure 3.16. The images of these three lenses are shown in Figure 3.17, Figure 3.18 and Figure 3.19. The focal length of each Fresnel lens versus the thickness of each image is given in Table 3.1 and Figure 3.20.

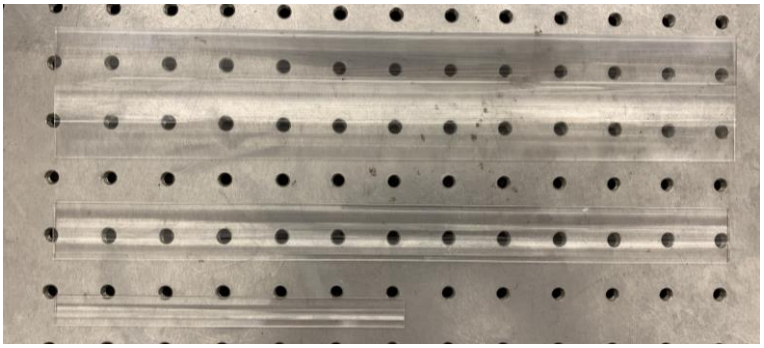

Figure 3.16 Three Different Sizes of Fresnel Lens. (From top to bottom, they are 5.72, 2.54 and 1.27 cm wide correspondingly)

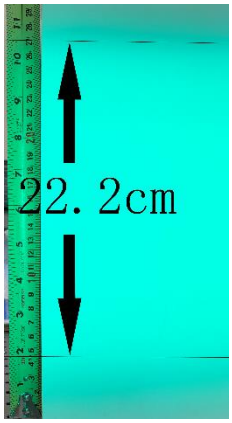

Figure 3.17 Image of 0.64 cm Focal Length Fresnel Lens

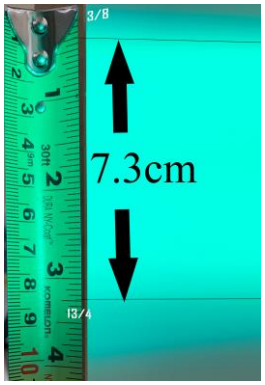

Figure 3.18 Image of 1.91 cm Focal Length Fresnel Lens

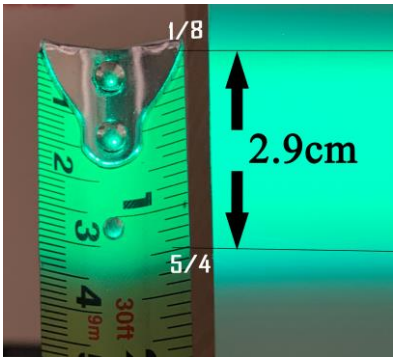

Figure 3.19 Image of 5.08 cm Focal Length Fresnel Lens

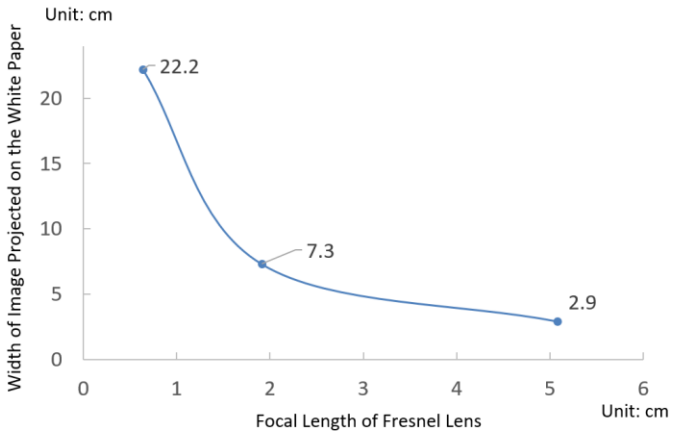

Figure 3.20 Focal Length of Fresnel Lens Vs Image Projected on White Paper

Table 3.1 Focal Length of Fresnel Lens Vs Width of Image

Focal Length of Fresnel Lens (cm)	0.64	1.91	5.08
Width of Image (cm)	22.2	7.3	2.9

From Figure 3.20, we can get that the thickness of light stripe decreases sharply at first, then the slope goes down very slowly. The thickness of the image is supposed to be as close to 2.54 cm as possible (this is the maximum thickness this equipment supposed to reach). Another consideration in selecting a lens is whether the box has enough space to accommodate the lens. The box is an 8.89 cm × 8.89 cm aluminum extrusion and the thickness of the wall is 0.64 cm. Hence, the 5.72 cm wide Fresnel lens is selected, of which the effective width is 5.08 cm, as the collimator.

3.4 Green Lantern 2.0 Design

The equipment is mainly divided into 4 parts: the heat sink assembly, the LED box assembly, the plastic sheets assembly and the electronics assembly. I will clarify each part in the following sections. The whole construction is shown in Figure 3.21.

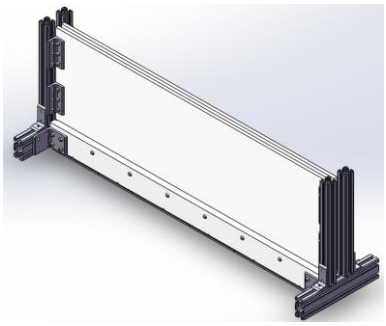

Figure 3.21 Green Lantern 2.0 Assembly

3.4.1 Heat Sink Assembly

The heat sink assembly consists of the heat sinks, LEDs on the heat sink, and the screws used to connect the LED box part. The heat sink used in this assembly is Alexandria Industries MM1220 of which the width is 8.89 cm and the heat transfer coefficient is 2.3 ℃/W which is based on 7.62 cm cut length in natural convection air flow.

In consideration of material thermal expansion as well as easy installation, the whole part is divided into 6 modules (20 cm long each module). The edge modules have 17 LEDs as in Figure 3.22 while the center modules have 19 LEDs each, as shown in Figure 3.23. The removal of 2 LEDs on the edge module is to avoid the intersection of the side wall and the LED. A 0.5 mm gap is left between neighboring LEDs in order to avoid thermal expansion.

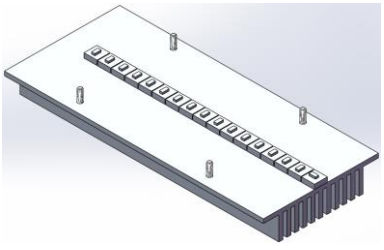

Figure 3.22 Edge Module

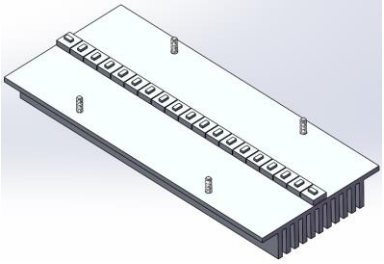

Figure 3.23 Center Module

3.4.2 LED Box Assembly

The LED box assembly consists of two 1.27 cm thick side walls (Figure 3.24), two half aluminum extrusions (Figure 3.25), one pair of lens holders (Figure 3.26) and four 5.72 cm wide Fresnel lenses (Figure 3.16).

As Figure 3.25 shows, the holes on the bottom of the aluminum extrusion are threaded holes in order to connect to the heat sink parts, which means the heat sink can be easily removed if it is broken. The half bare holes on the bottom are for the LED wires coming out to the specific LED drivers, the bare holes on the front surface are for the connection of the lens holders and the holes on the edge are used to connect the side walls. The final construction is shown in Figure 3.27; the 80/20 aluminum extrusions on both sides are for the connection of plastic sheet part.

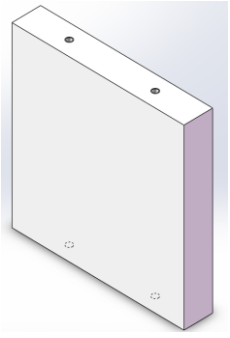

Figure 3.24 Side Wall

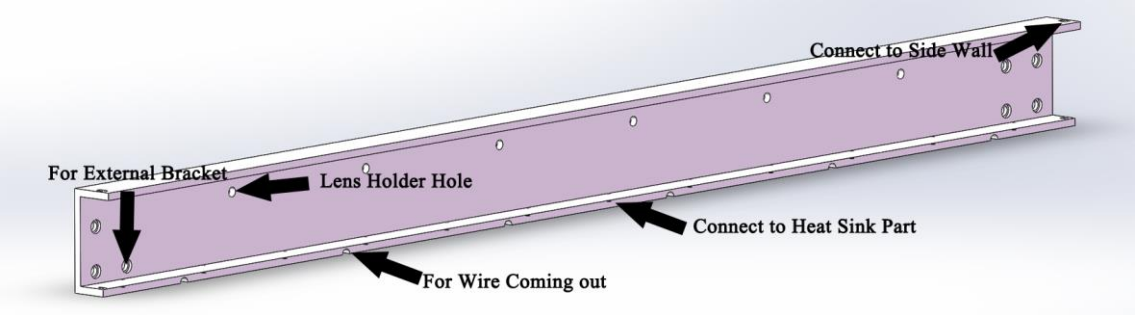

Figure 3.25 Aluminum Extrusion

Figure 3.26 Lens Holder

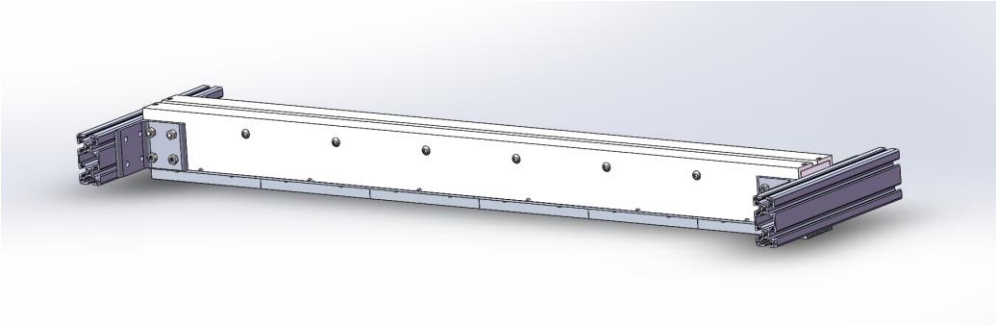

Figure 3.27 LED Box Part Assembly

3.4.3 Plastic Sheet Assembly

Each half of the assembly is shown in Figure 3.28 and consist of 6 brackets, two 39.37 cm long aluminum extrusions and a plastic sheet. The two bottom brackets are used to connect both sides of the assembly in Figure 3.27. This assembly acts as the baffle to cover non-parallel light, and the brackets on the bottom of this assembly are used to control the thickness of the light.

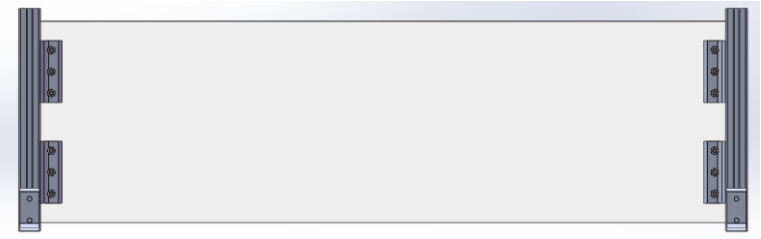

Figure 3.28 Plastic Sheet Part Assembly

3.4.4 Electronics Assembly

The LEDs chosen in this project need 700 mA current to illuminate. When working, the typical forward voltage is around 3V. So, a 700 mA constant current power supply is necessary. The power supply used is a Meanwell IDLC-45 (Figure 3.29), which can provide 700 mA constant current in the voltage range from 38V to 64V while the edge module needs 51 V and the center module needs 57 V. The whole circuit of the equipment is shown in Figure 3.30.

Figure 3.29 Meanwell IDLC-45 LED Power Supply

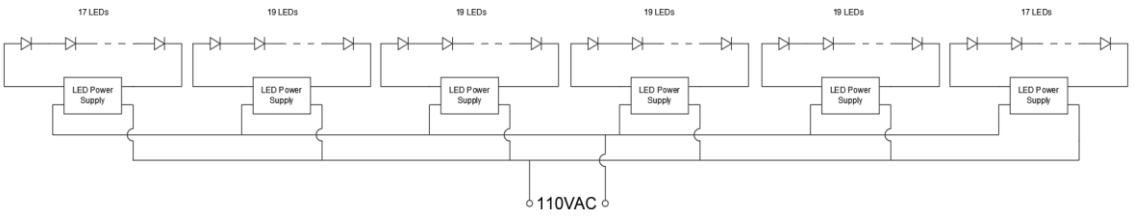

Figure 3.30 Electronic Part Circuit

3.5 Comparison of New and Old Green Lanterns

The aim of constructing the Green Lantern 2.0 is to provide a brighter light to illuminate the whole tank, the reason for this is that the high-speed camera has a very short exposure time, which means the exposure index of camera or the brightness of the particle in the water needs to be higher. However, the higher the exposure index is, the lower the fidelity of the image is. In order to get a clear picture, higher brightness is needed, which means higher brightness of illumination equipment is needed. The following sections will show the difference of old and new Green Lanterns.

3.5.1 Thickness of the Light Sheet

Since the thickness of the light sheet of Green Lantern 2.0 is changeable, in order to compare it with the old Green Lantern, the opening should be adjusted to the same width with the old one. However, the curvatures of the baffles of these two Green Lanterns are not same, and it is difficult to set the opening of the Green Lantern 2.0 the same as that of the original Green Lantern. To get the thickness at each test point, a transparent ruler is used, the ruler is set vertically to the light sheet. The value of the thickness of the light sheet is then read and recorded. There are five test points (shown in Figure 3.32) and each point is measured three times, the order of measurement is from the left edge to the right edge. Figure 3.31 (In order to avoid two error bars overlap each other, the points at 0% and 25% of the Green Lantern 2.0 are shifted to a little bit right) shows the

thickness of light sheet at the opening of Green Lantern and Green Lantern 2.0 (the comprehensive data are shown in Table B.7 and Table B.8 in Appendix B). The length of the light sheet of Green Lantern is 74.3 cm while the length of the version 2.0 is 120 cm and all measurements are tested at the points which are at the left edge, 25% of the whole length to the left, 50%, 75%, and the right edge of the opening, shown in Figure 3.32.

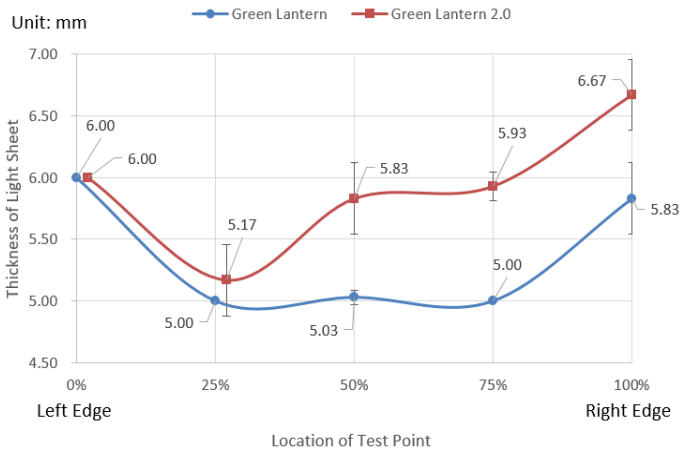

Figure 3.31 Thickness of Light Sheet at Opening of Both Green Lanterns. (Error bar shows standard deviation)

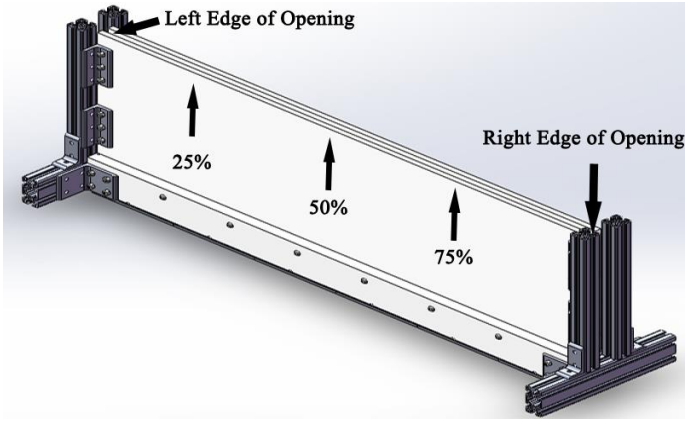

Figure 3.32 Test Points of Both Green Lanterns

To get the divergence angle for both Green Lanterns, the thicknesses of the light sheet at the same locations but 50 cm vertically higher than the opening are tested, the results are shown in Figure 3.33 (the comprehensive data are shown in Table B.5 and Table B.6 in Appendix B and in order to avoid overlapping, the 0%, 25% and 50% points of the Green Lantern 2.0 are shifted to right a little bit). The average numbers are selected to calculate the divergence angle, and Table 3.2 shows the divergence angles of each measured points for both Green Lanterns, the equation for calculating divergence angle (θ) is:

$$\theta = 2 \times \arctan\left(\frac{F - I}{2 \times 50cm}\right)$$

where F is the thickness of the light sheet at 50 cm higher than the opening and I is the thickness of the light sheet at the opening, shown in Figure 3.34

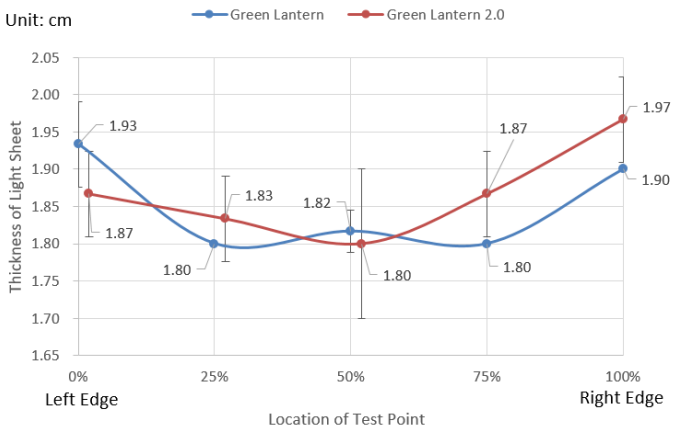

Figure 3.33 Thickness of Light Sheet at Points 50 cm Vertically away Opening of Both Green Lanterns. (Error bar shows standard deviation)

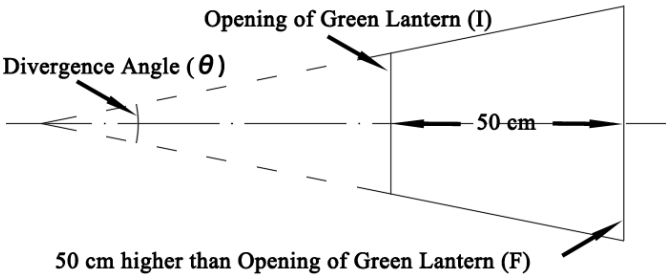

Figure 3.34 Sketch of Divergence Angle

Table 3.2 Divergence Angle for Both Green Lanterns

Location	0% (Left Edge)	25%	50%	75%	100% (Right Edge)
Green Lantern	1.52	1.49	1.51	1.49	1.51
Green Lantern 2.0	1.46	1.50	1.39	1.46	1.49

3.5.2 Brightness of the Light Sheet

The configuration of brightness test is the same as the one of the thickness test. The device used to test the brightness is Digital Illuminance Meter LX1330B, which is sensitive to green light and for which the error is less than 3%. This device measures in lux, which is a unit to quantify the amount of luminous flux in a unit area. All the values gotten in this experiment are the peak value at each point. To get the peak value, the device was set to peak value mode which will show the maximum value until it is cancelled, then slowly moved back and forth across the gap 2 to 3 times. The value was then recorded. Each point was measured three times. Figure 3.35 and Figure 3.36 show the brightness of the light sheet at both test points which are at the opening and 50 cm vertically higher than the opening (the comprehensive data are shown in Table B.1, Table B.2, Table B.3 and Table B.4 in Appendix B).

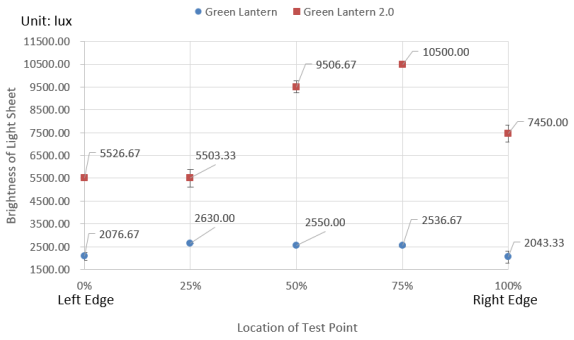

Figure 3.35 Brightness at Opening of Both Green Lanterns. (Error bar shows standard deviation)

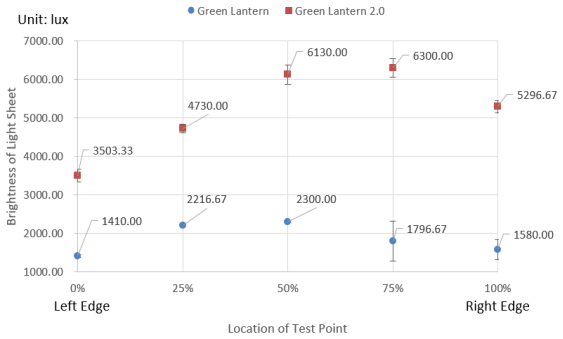

Figure 3.36 Brightness at 50 cm Higher than Opening of Both Green Lanterns. (Error bar shows standard deviation)

For the usage of the light of the Green Lantern 2.0, the brightness at the slot of the LED box is measured and compared with the brightness at the opening of the baffles when using the width shown in Table 3.3. The equation to calculate the efficiency is:

$$Efficiency = \frac{F}{O} \times 100\%$$

where O is the brightness at the opening of LED box (shown in Figure 3.37) and F is the brightness at the opening of the baffles (shown in Figure 3.38). The efficiency is shown in Table 3.5. The table shows that approximately 5% of the total produced light is used to form the emitted light sheet.

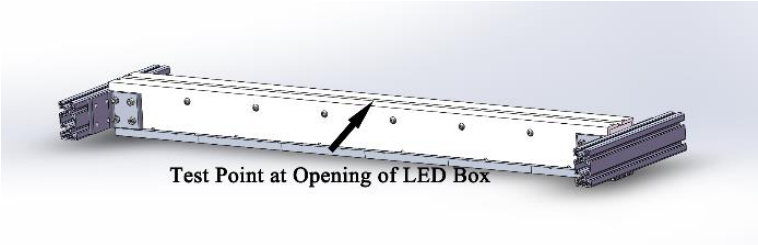

Figure 3.37 Test Point at Opening of LED Box

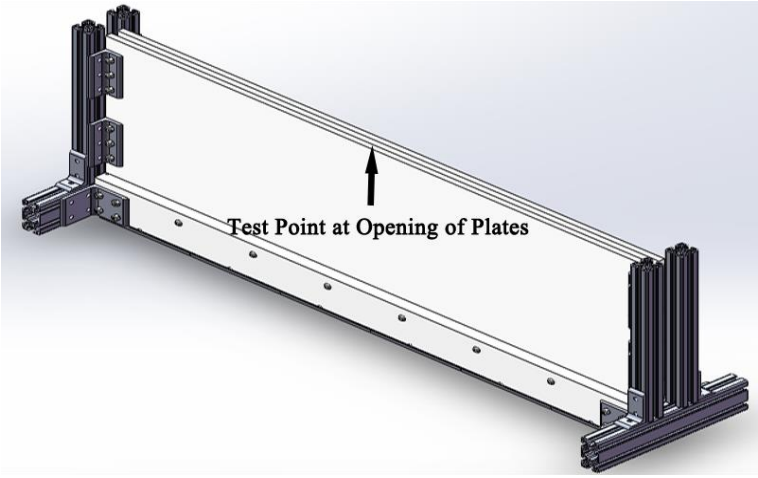

Figure 3.38 Test Point at Opening of Baffles

Table 3.3 Efficiency of Green Lantern 2.0

Unit: Lux	Left	Center	Right
At the opening of LED Box	$1.369*10^5$	$1.796*10^5$	$1.322*10^5$
At the opening of the Baffles	$5.52667*10^3$	$9.50667*10^3$	$7.45*10^3$
Efficiency	4.04%	5.29%	5.63%

Figure 3.39 and Figure 3.40 are two images captured by the high-speed camera, both of them are captured using the same configuration – resolution: 2560 × 1600, exposure time: 41000µs, exposure index: 32000, and f-stop: 1.8. Figure 3.41 and Figure 3.42 are the distributions of the brightness of each pixel in both images.

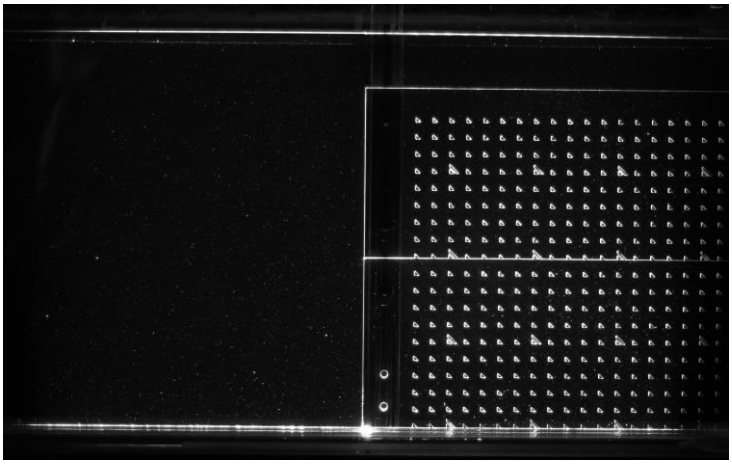

Figure 3.39 Image Captured Using Green Lantern

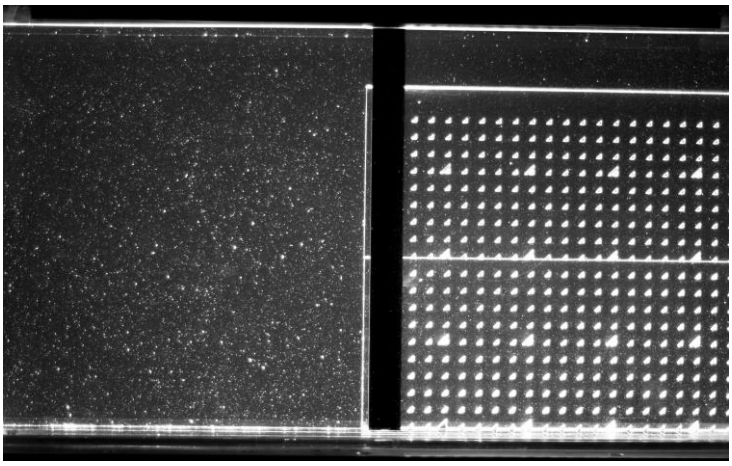

Figure 3.40 Image Captured Using Green Lantern 2.0

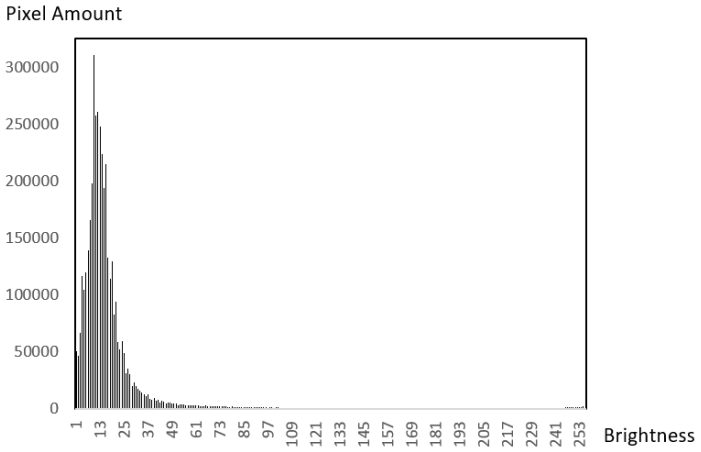

Figure 3.41 Histogram of Image Captured Using Green Lantern

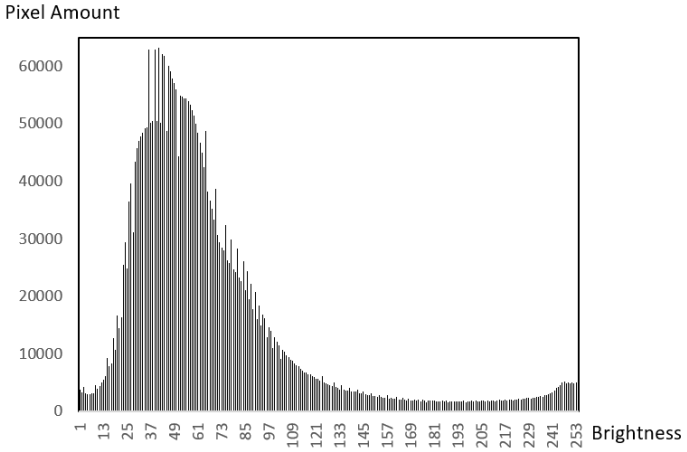

Figure 3.42 Histogram of Image Captured Using Green Lantern 2.0

With the original Green Lantern, the majority of pixels distribute in a sharp shape of which the peak is at the brightness of 9 and the amount of pixels at that brightness is 310960, which means most of pixels are at a relatively low brightness. The histogram of the image with Green Lantern 2.0 is more even distributed than the old one and the peak is at the value of 41 where there are 63201 pixels and the brightness of majority of pixels is in the range from about 13 to about 121, which means majority of pixels are much brighter than Green Lantern. From this comparison,

it is obvious that Green Lantern 2.0 can illuminate more particles (because it is longer than Green Lantern) as well as with a higher brightness.

3.6 Thermal Performance of Both Green Lanterns

The maximum operating temperature of the LED used in the Green Lantern 2.0 is 135 ℃. This section shows the relation between time and temperature to make sure the Green Lantern can run in a safe temperature range. The test point is selected at the center of the heat sink (shown in Figure 3.42 and the comprehensive data are shown in Table B.9 in Appendix B) and the relation between temperatures of this point and time is shown in Figure 3.43. The ambient temperature during the experiment is 20.6℃.

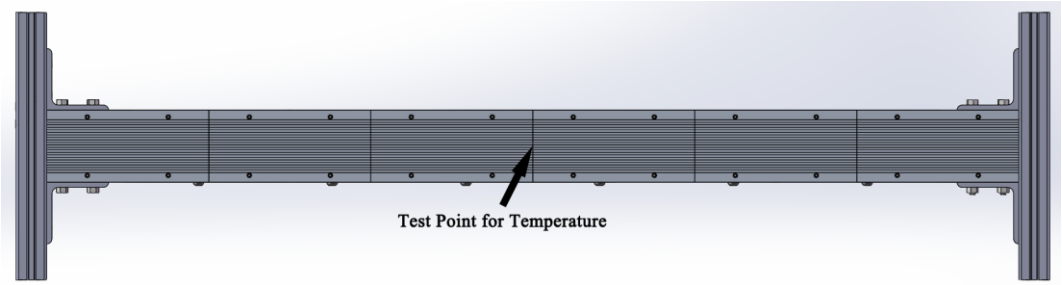

Figure 3.43 Test Point for Temperature

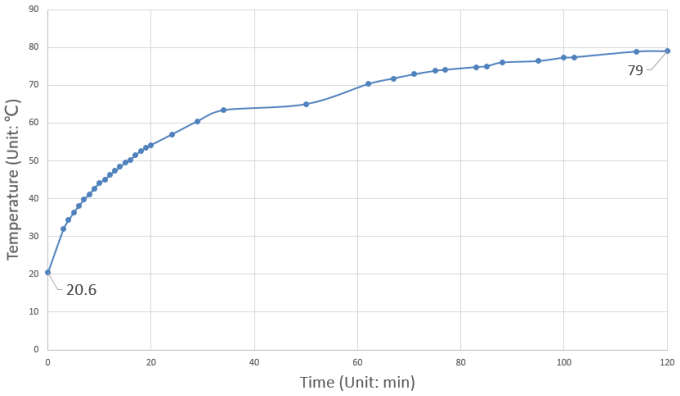

Figure 3.44 Temperature of Heat Sink Vs Time for Green Lantern 2.0

From Figure 3.43, the temperature increases rapidly in the first 20 minutes and gradually slows down, in the last half duration the temperature increases less than 20℃ and increases less than 2℃ in the last 20 minutes. Finally, it reaches equilibrium around 79℃, which is less than 135℃. Although the temperature stops increasing at 79℃, the difference (about 59℃) between original and final temperature causes other problems, which will be discussed in next section.

The temperature of original Green Lantern is also tested as a comparison with the new one, Figure 3.45 is the temperature vs time for the original Green Lantern (The comprehensive data is shown in Table B.10 in Appendix B). Comparing with the new Green Lantern, the old one uses a longer time to reach the temperature equilibrium, which is after 150 mins. The max temperature it can reach is 48.1℃ (ambient temperature is 21.2℃) while the Green Lantern 2.0 is 79℃ (20.6℃).

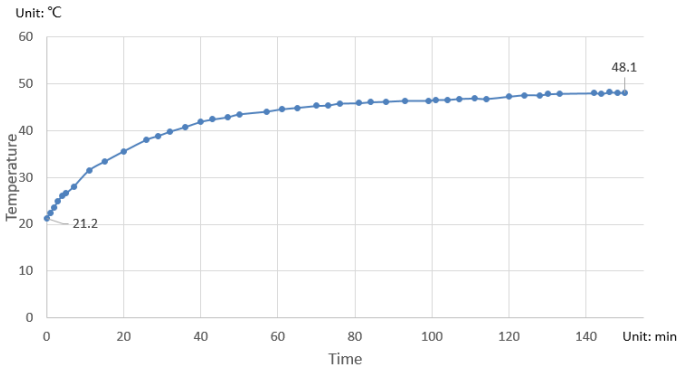

Figure 3.45 Temperature of Heat Sink Vs Time for Original Green Lantern

3.7 Discussion

The thickness and brightness of both Green Lanterns are completely compared in section 3.5 and the thermal performance of the Green Lantern 2.0 is also shown in section 3.6. It is obvious that the aim of the Green Lantern 2.0 has been reached. From Figure 3.34 and Figure 3.35, the brightness of the Green Lantern 2.0 is about 2 times to 4 times of the one of the Green Lantern

varying by different test points. From Figure 3.40 and Figure 3.41, the peaks of two histograms are 9 and 41 for the Green Lantern and the Green Lantern 2.0 respectively, and this result corresponds the one measured from the illuminance meter.

For the measurement of the light sheet, the gap of the opening of the Green Lantern 2.0 is adjusted to be as close to the one of the Green Lantern as possible, which means the gaps (6 mm wide) of the opening of the Green Lantern 2.0 at the left and right edge are same as the one of the Green Lantern. However, the gap will change as the temperature of the LED box increases. As the temperature increases, the aluminum (the material of the LED box) as well as the plastic (the material of the baffles) will suffer thermal expansion, which may make the baffles open and close a little bit varying through the lengthwise direction. The order to measure the test point in all experiments is testing from the left edge to the right edge of both Green Lanterns, and finishing one round will take about 5 mins. This might be the reason why the thickness at the right edge in Figure 3.31 is 0.67 mm (ignoring the measurement error) larger than the left edge. Further, the brightness of the Green Lantern at the right edge is higher than the left edge one, shown in Figure 3.34 and Figure 3.35. The brightness seems to increase with the width of the gap increases, but this needs to be determined whether the brightness of the light sheet increases as the width of the gap increases or as the time lapses, because it seems that the brightness of LED is increasing when the temperature is increasing.

CHAPTER 4: EXPERIMENT USING PIV

4.1 Introduction

PIV is particle image velocimetry, developed in 1980s, used to work in the field of laser speckle photography. During that time, without the help of digital image technology as well as advanced high speed camera, the whole process including the setup of equipment, the process of film and the evaluation of photos cost a lot of time in the past [19]. However, with the modern computer and camera technology, this process becomes much easier and faster.

The applications of PIV span many aspects such as wind tunnel velocity experiments, velocity measurements in fluid and environmental research. For example, Steven and Sean et al studied compressible turbulence flow in a high speed wind tunnel by using the mean of pulse-burst PIV [20]. Foeth and Van et al gave the visualization and analyzation of the 3D sheet cavitation on the hydrofoil by using Time Resolved Particle Image Velocimetry (TRPIV) [21]. Wagner and Casper et al get the relationship between acoustic tones and flow structure in transonic cavity flow by time resolved PIV [22]. Meinhart and Wereley et al studied and described another way to measure a microchannel flow by PIV with 200 nm diameter flow-tracing particles in order 1-μm spatial resolution [23]. There are several kinds of PIV setups in order to meet different purposes such as 2D PIV, stereo PIV, 3D PIV and micro PIV etc. The aim of this paper is based on 2D Langmuir Circulation flow, so 2D PIV will be used in this chapter. Since the Green Lantern 2.0 is finished after this experiment and there is too short time to redo the experiment, the original Green Lantern is used in this chapter.

4.2 Experiment Setup

Generally, the experiment includes the following facilities:

(1) Acrylic tank: the reservoir for the water and tracers, the dimension is 1 m long × 0.2 m wide × 0.5 m deep.

(2) Conveyor belts, shafts and motors: used to force the fluid motion, the motors can provide multiple rotation speeds and run in clockwise and anti-clockwise directions.

(3) Tracer: because of the transparency of water, tracer is needed in this experiment for the flow to be captured by camera.

(4) High speed camera: used to get images for analysis after the experiment.

(5) High power LED light: use to provide enough brightness for the camera to capture the image.

The layout of these facilities is shown in Figure 2.1, the high speed camera is placed in the center of the front wall of the tank. The distance between the front wall of the tank and the lens of the camera is 1.58 m.

The main purpose of this experiment is to see the velocity field of the water in the tank at different speeds and rotation directions of the conveyor belt. The experiment can be divided into the following steps:

(1) Add tracer into the water to make the flow of water visible.

(2) Make the high speed camera focus on the light sheet.

(3) Put a calibration plate into the water in order to know the relation between the distance in the real world and in the image.

(4) Input the parameters to control the motor in order to drive the water flow.

(5) Stir the water in order to refloat the tracers and make the water flow random.

(6) Start the conveyor belts to drive the motion of the fluid.

(7) Wait until the water flow becomes stable.

(8) Capture an image sequence.

(9) Redo step (4) with different parameters till finish the image data collection.

(10) Calibrate the raw images captured in step (7) with PIV software.

(11) Analyze the calibrated images with PIV software.

For the parameters in step (4), the original motor step size is 1.8 degree. The resolution of the motor is set to 4, which means one original step is divided into 4 small steps. So, one step is 0.45 degree. 700 steps/s, 1400 steps/s, 2100 steps/s, 2800 steps/s and 3500 steps/s are used in this experiment and the circumference of the shaft is 6.35 cm, so the input velocities of the conveyor belts are 17.46 cm/s, 34.92 cm/s, 52.38 cm/s, 69.84 cm/s and 87.30 cm/s respectively. All PIV measurements and analysis were conducted in conjunction with Dr. Carlowen Smith.

4.3 Results and Conclusion

Figure 4.1 and Figure 4.2 are the time mean velocities for 700-3500 steps/s of both upwelling and downwelling direction. It can be concluded that overall, the experimental setup can successfully create two counter-rotating vortices at different speeds and directions.

However, there are some differences between different experimental parameters. In the downwelling flow, the vortices happen closer to the top of the tank. From Figure 4.1, the vortices happen among the top 1/2 of the total water and the right vortex becomes large and less coherent as the speed of the fluid increases. Also, the area of convergence moves to the left as the speed is increased.

For the upwelling flow, the converging area nearly does not change with the speed of the fluid, it always happens at $x \approx 38$cm. The location and size of the vortices, which occupies 3/5 to

4/5 of the tank, are nearly constant. With the comparison of these images, it can be concluded that the vortices are most clear and distribute most evenly at the lowest speed and upwelling flow.

Figure 4.3 shows the mean fluid speed vs. the speed of the conveyor belts. The mean fluid speed generally increases as the conveyor belt speed increases. However, when the speed of the conveyor belt is at the maximum, which is 3500 steps/s, the mean velocity of the water drops down, this may be caused by the failure of the motor. When the motor tries to get 3500 steps/s, the force is too much to sustain at that rate of steps, then the actual speed of conveyor belt goes down, consequently causing the mean velocity of the water drops down.

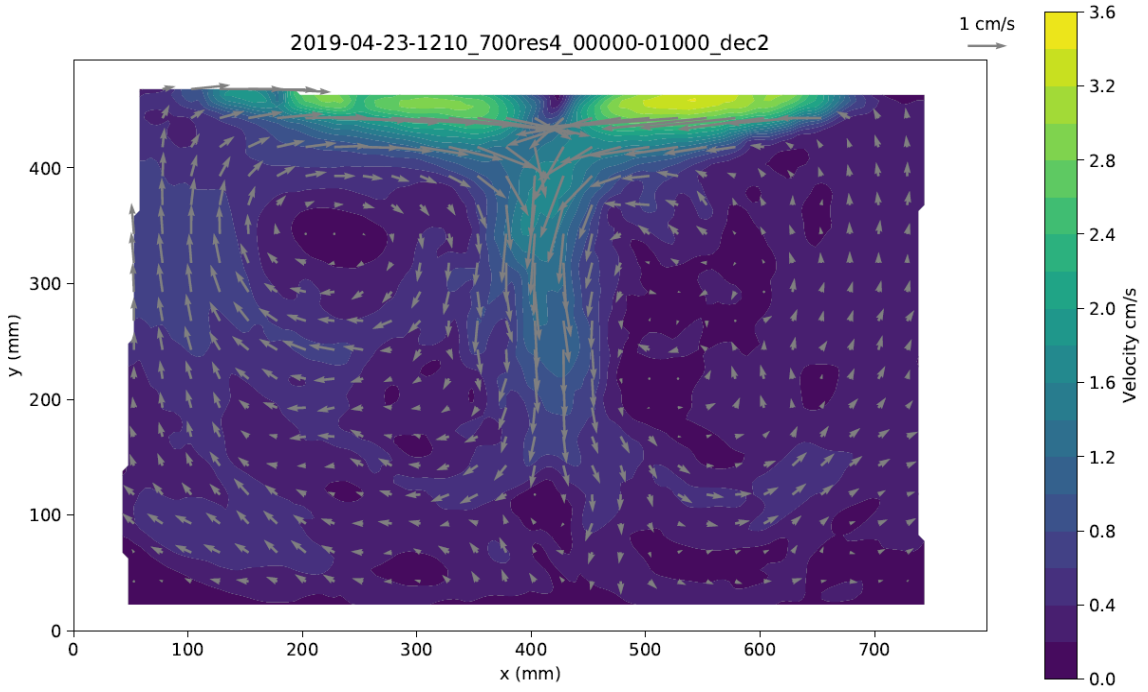

(a) Belt Speed: 17.46 cm/s (700 steps/s)

Figure 4.1 Mean Velocity for Downwelling Flow [24]

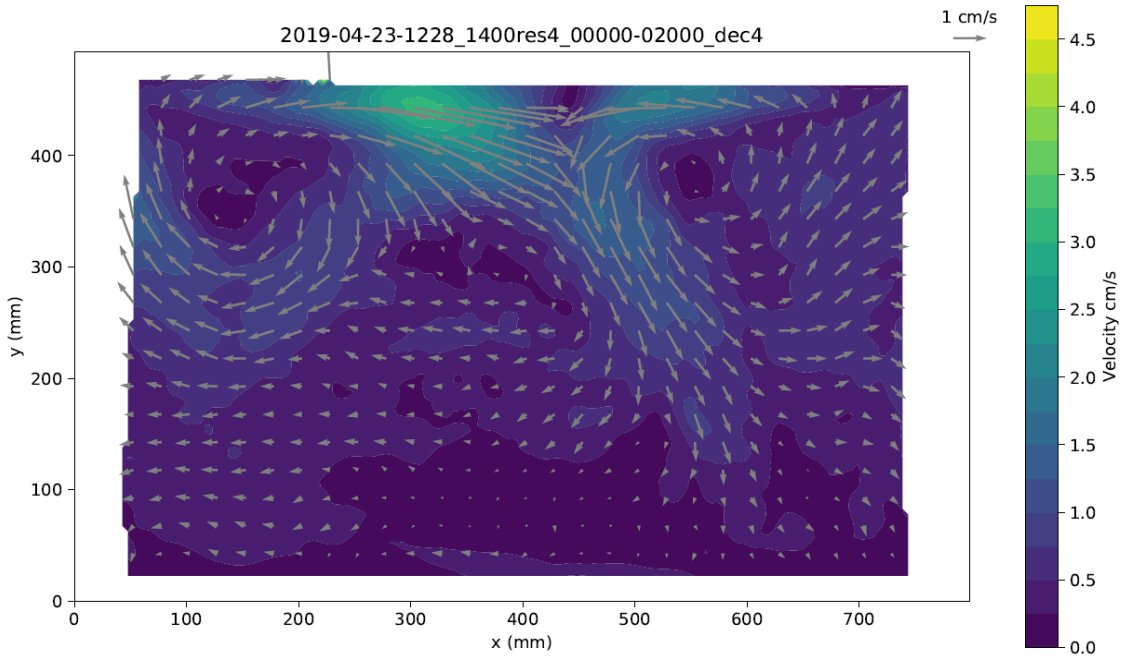

(b) Belt Speed: 34.92 cm/s (1400 steps/s)

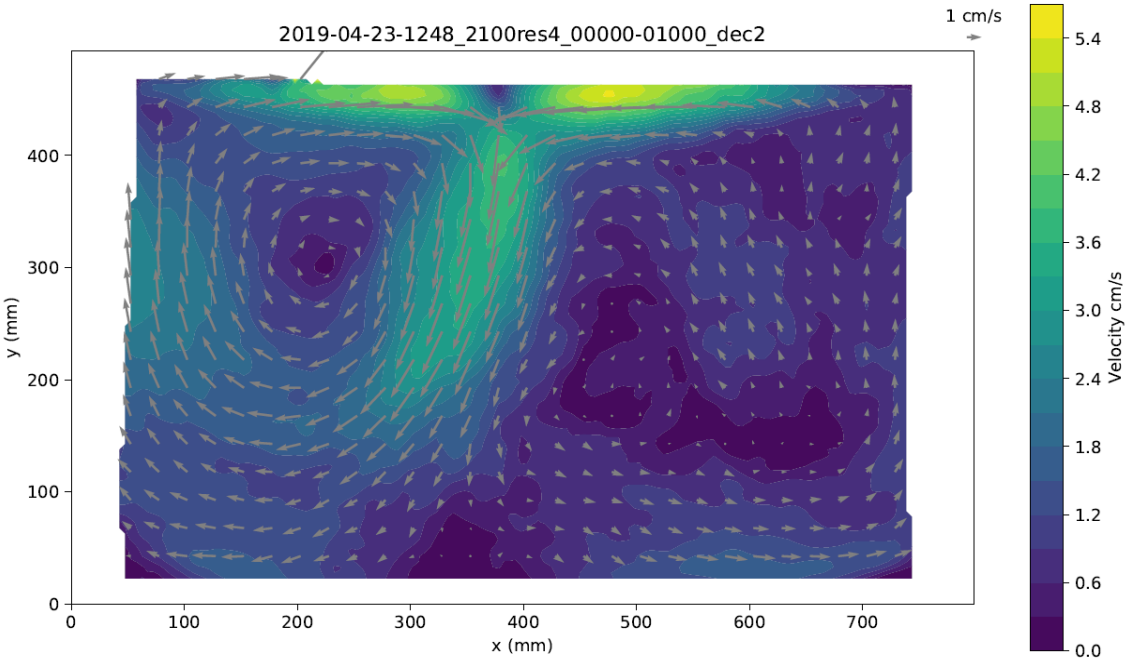

(c) Belt Speed: 52.38 cm/s (2100 steps/s)

Figure 4.1 (Continued)

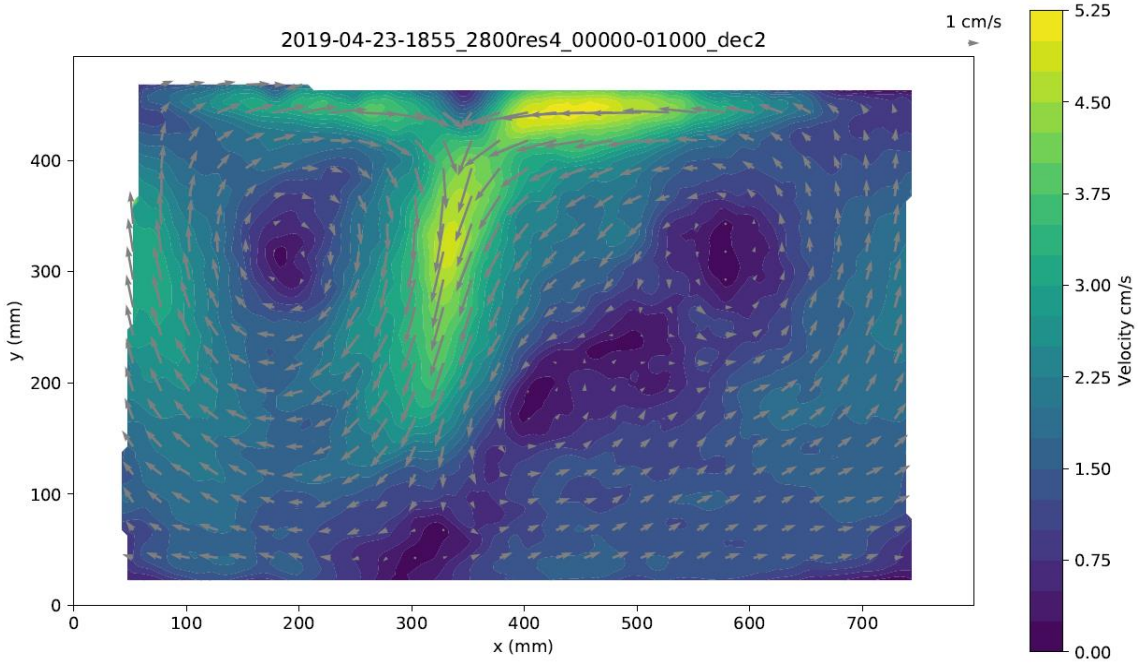

(d) Belt Speed: 69.84 cm/s (2800 steps/s)

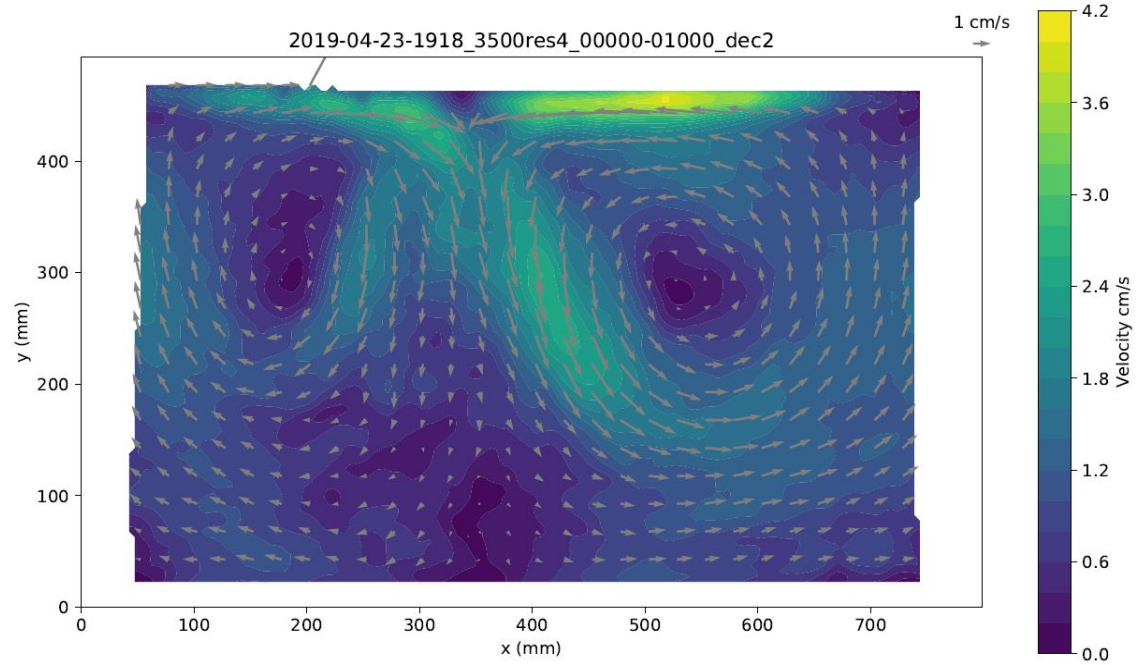

(e) Belt Speed: 87.30 cm/s (3500 steps/s)

Figure 4.1 (Continued)

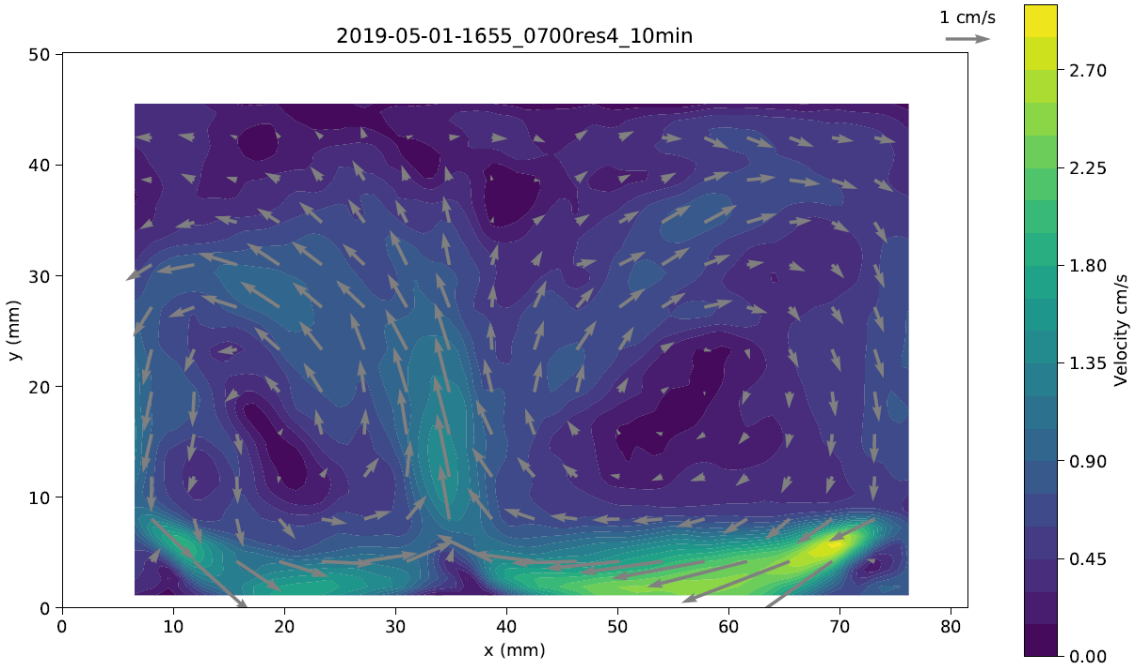

(a) Belt Speed: 17.46 cm/s (700 steps/s)

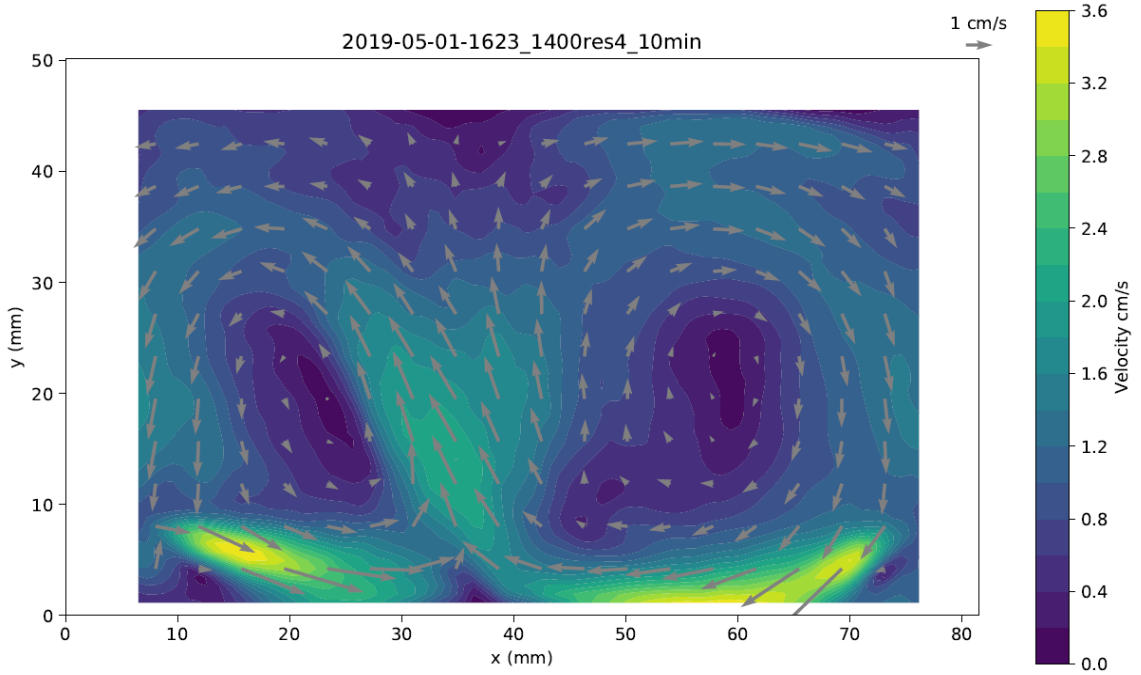

(b) Belt Speed: 34.92 cm/s (1400 steps/s)

Figure 4.2 Mean Velocity for Upwelling Flow [24]

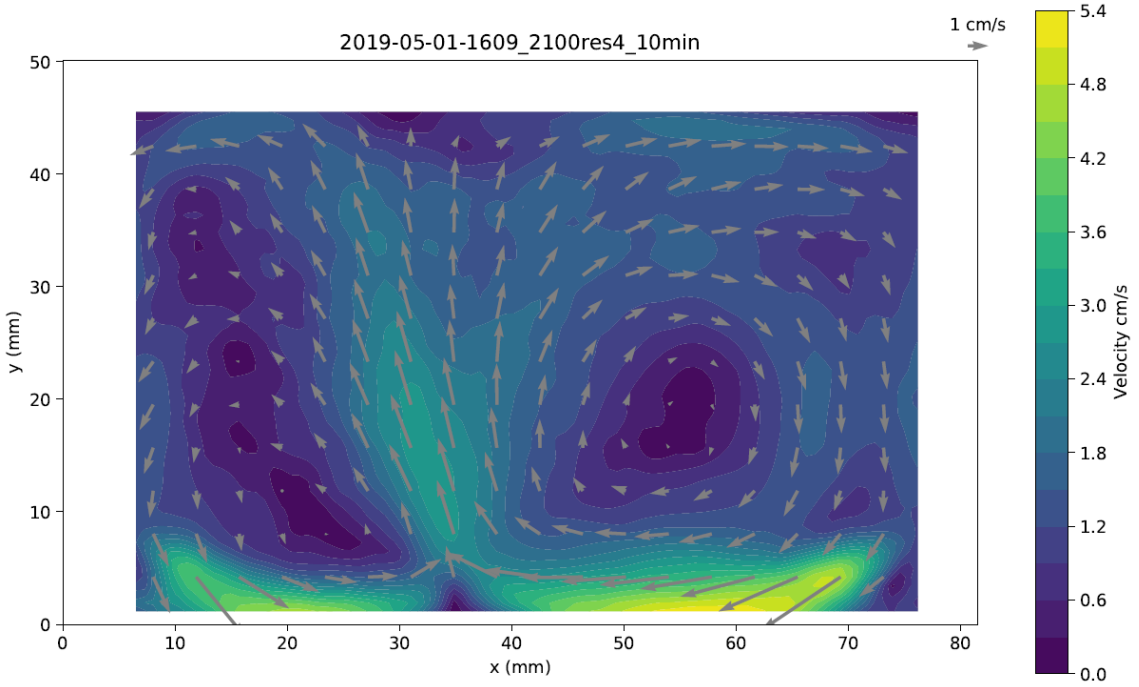

(c) Belt Speed: 52.38 cm/s (2100 steps/s)

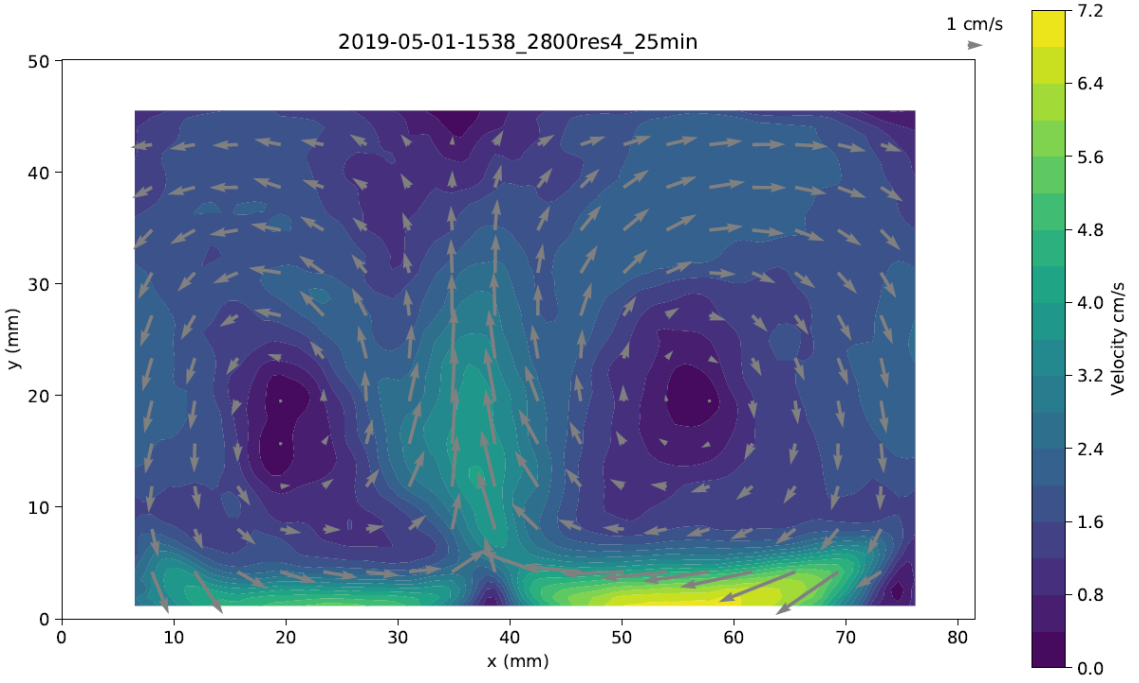

(d) Belt Speed: 69.84 cm/s (2800 steps/s)

Figure 4.2 (Continued)

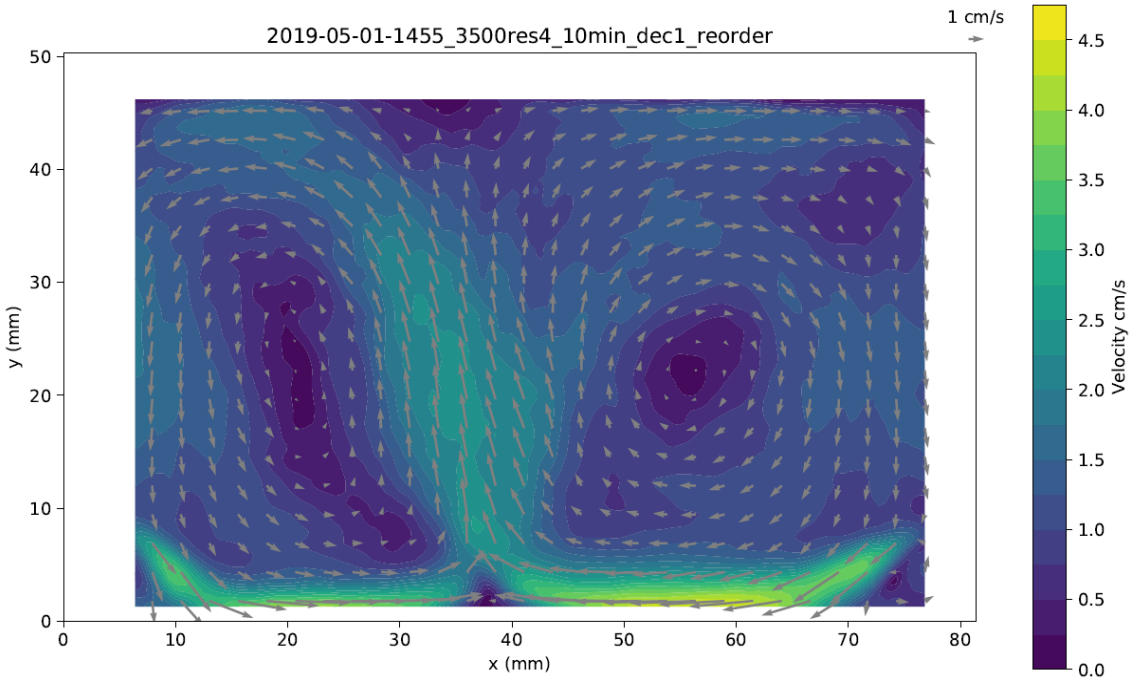

(e) Belt Speed: 87.30 cm/s (3500 steps/s)

Figure 4.2 (Continued)

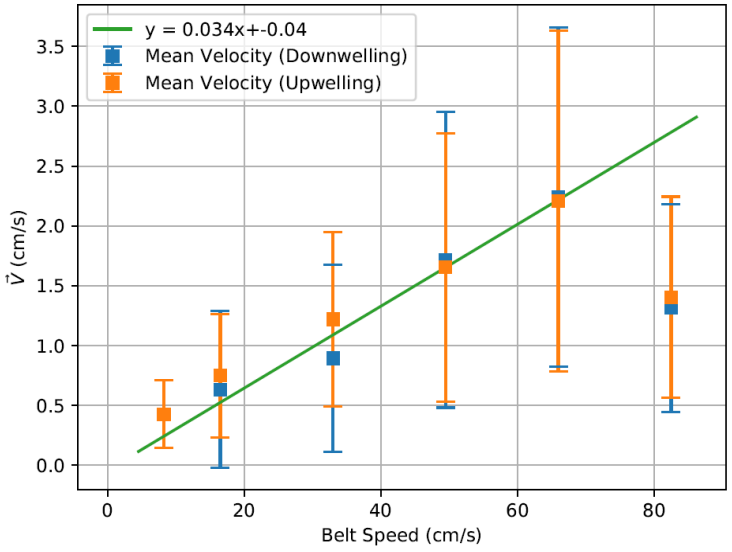

Figure 4.3 Mean Velocity of Water Vs Speed of Conveyor Belt [24]. (Error bars indicate standard deviation. Fit is shown for experiments with belt speeds below 80 cm/s)

CHAPTER 5: CONCLUSION AND FUTURE WORK

This thesis mainly discusses the design and testing of the Langmuir Circulation experimental facility. Chapter 2 describes the testing of the acrylic tank by ANSYS, providing information about the deformation, equivalent stress, and safety factor when the tank is 1/4, 1/2, 3/4 and full of water. We found that when the water is more than 1/2 of the tank, the deformation is so large that the distortion of the image captured by camera cannot be ignored. So, a brace is added on the top of the tank for which the optimized distance between the two short beams is analyzed as 0.55 times the length of the long beam. The real images of the tank with and without the clamp on are also shown in this chapter.

Chapter 3 focuses on the design of the Green Lantern 2.0 to be used in experiments with the Langmuir Circulation facility. This chapter explains in detail every subassembly of the Green Lantern 2.0 and the process for choosing proper LED emitters and lenses. This chapter also includes a comparison with the old Green Lantern in terms of the thickness and brightness of the resulting light sheet. In order to have a line shaped light sheet, only one row of emitters is necessary, otherwise the image will show more than one line. For the selection of the kind and size of the focusing lens, the 5.72 cm wide Fresnel lens is chosen, which is easy to hold, occupies less space and performs the best. As to the comparison of the old and new Green Lanterns, the brightness of the new one is about 2 to 4 times of the brightness of the old one. The thickness of the new one is changeable while the old one is not and the Green Lantern 2.0 can illuminate the target field more evenly than the old one.

Chapter 4 discusses test runs of the experiment with PIV, with different speed and direction of conveyor belt motion to create different flows in the tank. For the motion, 700 steps/s, 1400 steps/s, 2100 steps/s, 2800 steps/s and 3500 steps/s which are equal to 17.46 cm/s, 34.92 cm/s, 52.38 cm/s, 69.84 cm/s and 87.30 cm/s respectively are used in this experiment. For the direction, there are two cases: one is that the fluid meets at the center of the bottom of the tank and flows up, the other one is that the fluid meets at the center of the water surface and flows down. After analyzing with DaVis software (LaVision, Inc.), it can be concluded that at lower velocities of the conveyor belt, the vortices in the tank are clearer. Besides, the results also show that the upwelling flow is more stable than the downwelling flow. When the motor runs at 3500 steps/s, it may not have enough force to drive the conveyor belt so that the speed of the water is less than the case with 2800 steps/s.

Future work for the simulation of the experiment tank would be to do more simulations with cross beams at positions 0.25 and 0.75 times of the length of the long beam to get a more accurate trend of total deformation. For the Green Lantern 2.0, it would be good to get the relation between the brightness of LED vs time to make sure whether the brightness of LED will increase as the time lapses. If so, the Green Lantern can be preheated for a certain duration to get the best performance; if not, then we can make sure the change in the brightness of the Green Lantern 2.0 in section 3.5.2 is only caused by the thermal expansion. To reduce the thermal expansion, one way is to lift the baffles a little bit to avoid the material of the baffles directly touching the hot aluminum surface. In addition, the curvature of the baffles can be reduced by adding two long beams at the top and bottom edges of the baffles which can brace the baffles to increase their rigidity and prevent bending.

REFERENCES

[1] Bainbridge, R. (1957). The size, shape and density of marine phytoplankton concentrations. Biological Reviews, 32(1), 91-115.

[2] Langmuir, I. (1938). Surface motion of water induced by wind. Science, 87(2250), 119-123.

[3] Smith, J. A. (1992). Observed growth of Langmuir circulation. Journal of Geophysical Research: Oceans, 97(C4), 5651-5664.

[4] Thorpe, S. A. (2004). Langmuir circulation. Annu. Rev. Fluid Mech., 36, 55-79.

[5] Weller, R. A., & Price, J. F. (1988). Langmuir circulation within the oceanic mixed layer. Deep Sea Research Part A. Oceanographic Research Papers, 35(5), 711-747.

[6] Weller, R. A., Dean, J. P., Price, J. F., Francis, E. A., Marra, J., & Boardman, D. C. (1985). Three-dimensional flow in the upper ocean. Science, 227(4694), 1552-1556.

[7] Smith, J., Pinkel, R., & Weller, R. A. (1987). Velocity structure in the mixed layer during MILDEX. Journal of physical oceanography, 17(4), 425-439.

[8] Buranathanitt, T., 1979. Some effects of Langmuir circulation on suspended particles in lakes and reservoirs. Ph.D. Thesis, Leicester University Engineering Department, England, Chapter 1.

[9] Stewart, R. H. (2008). Introduction to physical oceanography (pp. 133-147). College Station: Texas A & M University.

[10] Gargett, A.E., J.R. Wells, A.E. Tejada-Martinez and C.E. Grosch (2004) "Langmuir supercells: A dominant mechanism for sediment resuspension and transport", Science, 306, 1925-1928.

[11] Dethleff, Dirk, and E. W. Kempema. "Langmuir Circulation Driving Sediment Entrainment into Newly Formed Ice: Tank Experiment Results with Application to Nature (Lake Hattie, United States; Kara Sea, Siberia)." Journal of Geophysical Research 112, no. C2 (2007). doi:10.1029/2005jc003259.

[12] Chiba, David, and Burkard Baschek. "Effect of Langmuir Cells on Bubble Dissolution and Air-sea Gas Exchange." Journal of Geophysical Research 115, no. C10 (2010). doi:10.1029/2010jc006203.

[13] Hamner, W. M., & Schneider, D. (1986). Regularly spaced rows of medusae in the Bering Sea: Role of Langmuir circulation 1. Limnology and Oceanography, 31(1), 171-176.

[14] Barstow, S. F. (1983). The ecology of Langmuir circulation: a review. Marine Environmental Research, 9(4), 211-236.

[15] Buchmann, N. A., Willert, C. E., & Soria, J. (2012). Pulsed, high-power LED illumination for tomographic particle image velocimetry. Experiments in fluids, 53(5), 1545-1560.

[16] Estevadeordal, J., & Goss, L. (2005, January). PIV with LED: particle shadow velocimetry (PSV) technique. In 43rd AIAA aerospace sciences meeting and exhibit (p. 37).

[17] Bröder, D., & Sommerfeld, M. (2007). Planar shadow image velocimetry for the analysis of the hydrodynamics in bubbly flows. Measurement Science and Technology, 18(8), 2513.

[18] Macka, M., Piasecki, T., & Dasgupta, P. K. (2014). Light-emitting diodes for analytical chemistry. Annual Review of Analytical Chemistry, 7, 183-207.

[19] Raffel, Markus, et al. Particle image velocimetry: a practical guide. Springer, 2018.

[20] Beresh, S. J., Kearney, S. P., Wagner, J. L., Roy, S., Jiang, N., Slipchenko, M. N., ... & Mance, J. (2015). Pulse-burst PIV in a high-speed wind tunnel. In 53rd AIAA Aerospace Sciences Meeting (p. 1218).

[21] Foeth, E. J., Van Doorne, C. W. H., Van Terwisga, T., & Wieneke, B. (2006). Time resolved PIV and flow visualization of 3D sheet cavitation. Experiments in Fluids, 40(4), 503-513.

[22] Wagner, J. L., Casper, K. M., Beresh, S. J., Pruett, B., Spillers, R., & Henfling, J. (2015). Relationship between acoustic tones and flow structure in transonic rectangular cavity flow. In 45th AIAA Fluid Dynamics Conference (p. 2937).

[23] Meinhart, C. D., Wereley, S. T., & Santiago, J. G. (1999). PIV measurements of a microchannel flow. Experiments in fluids, 27(5), 414-419.

[24] Carlowen Smith, personal communication, May 20, 2019

APPENDIX A: TANK SIMULATION RESULTS

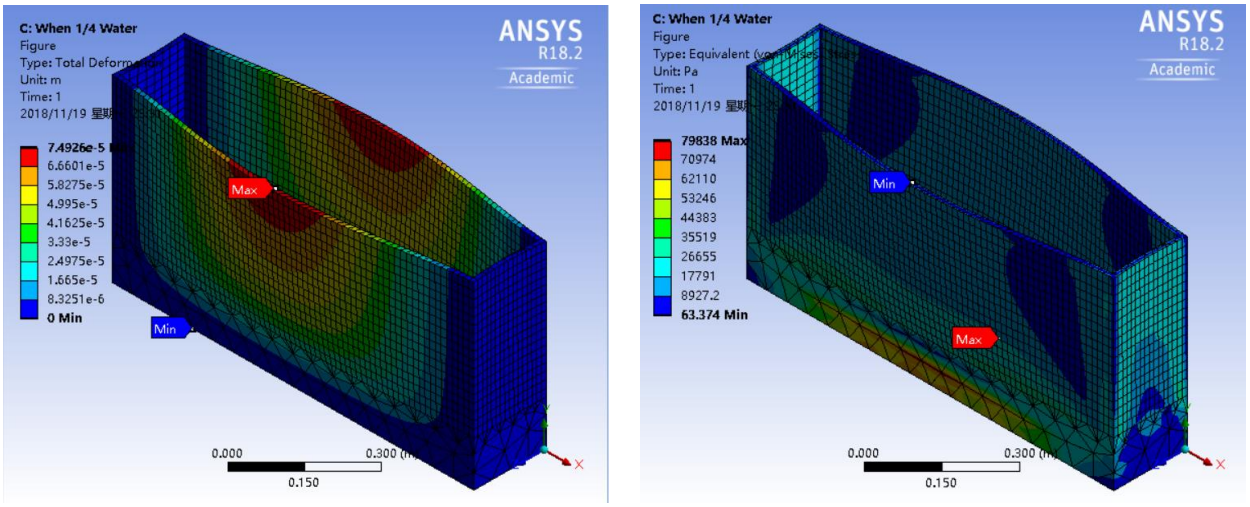

(a) (b)

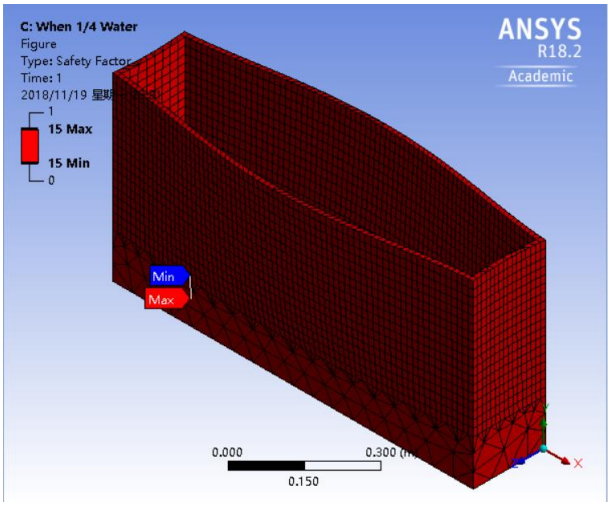

(c)

Figure A.1 1/4 Water Tank Results. (a. Total Deformation, b. Equivalent Stress, c. Safety Factor)

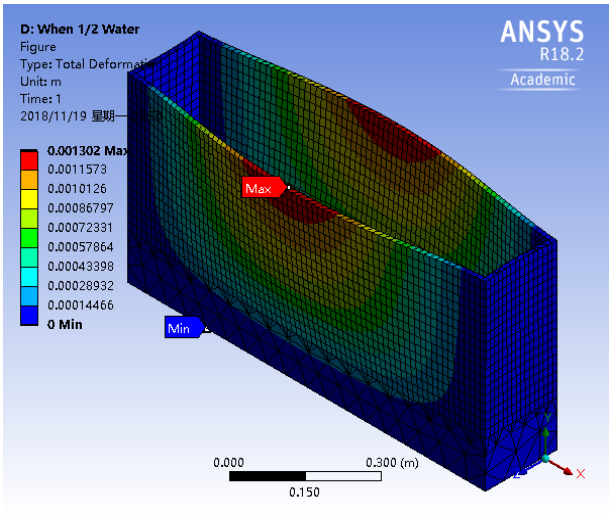

(a)

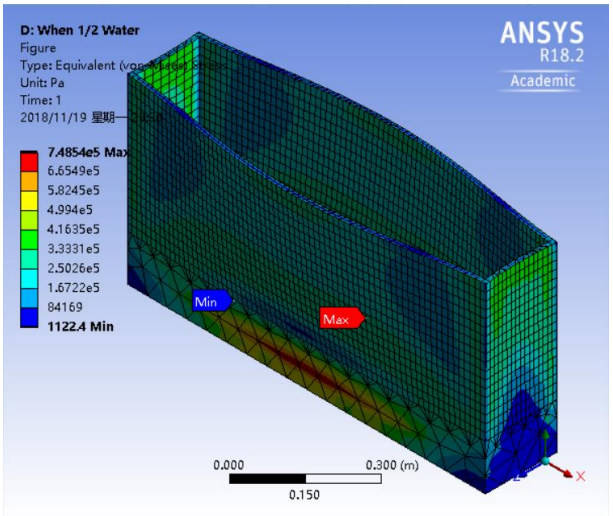

(b)

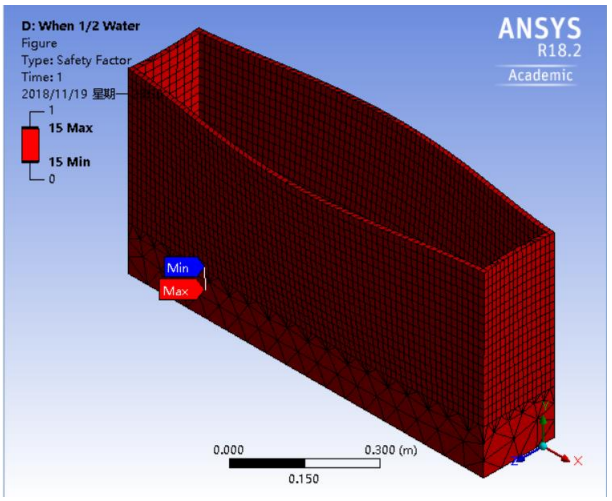

(c)

Figure A.2 1/2 Water Tank Results. (a. Total Deformation, b. Equivalent Stress, c. Safety Factor)

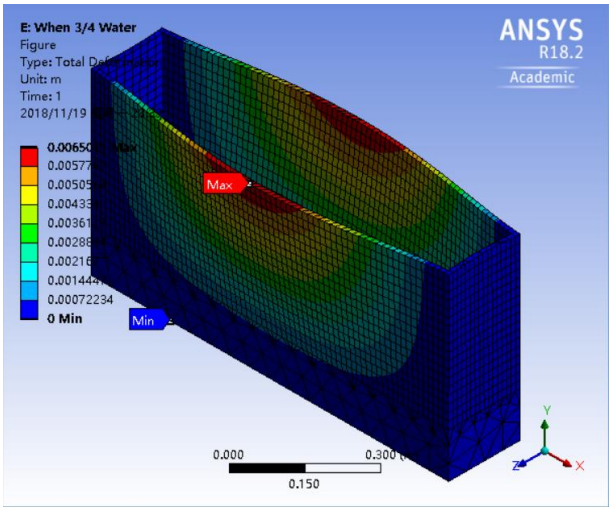

(a)

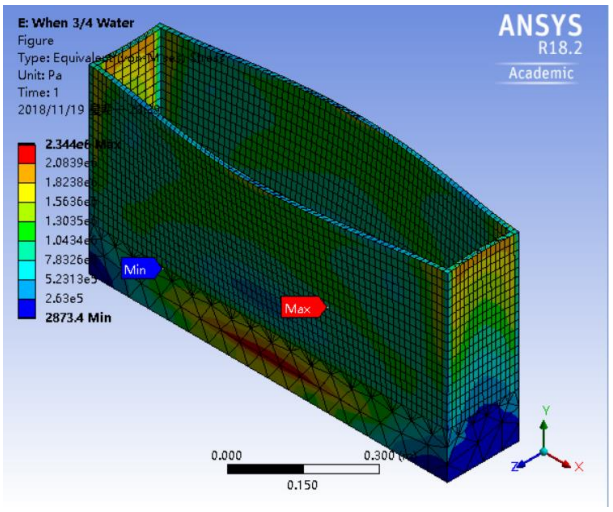

(b)

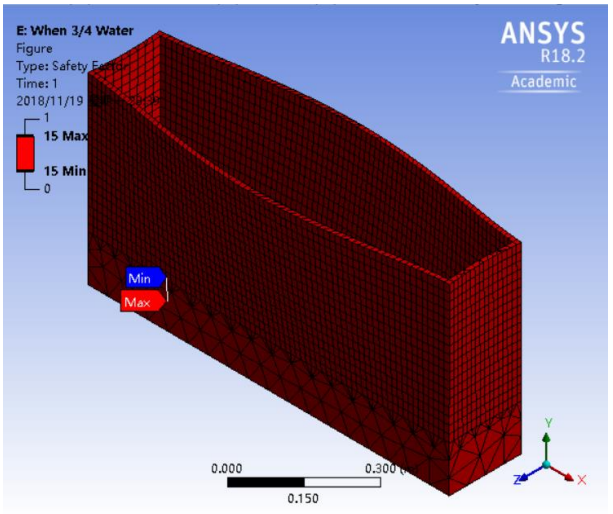

(c)

Figure A.3 3/4 Water Tank Results. (a. Total Deformation, b. Equivalent Stress, c. Safety Factor)

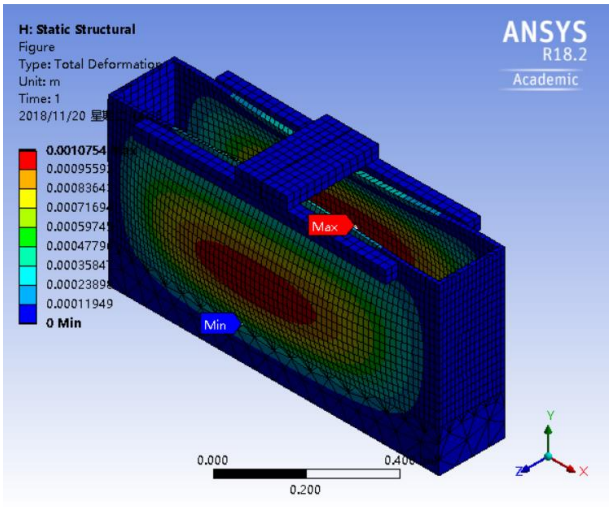

(a)

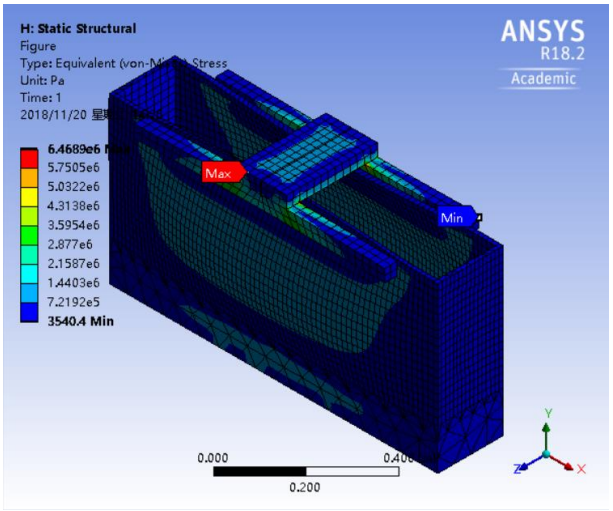

(b)

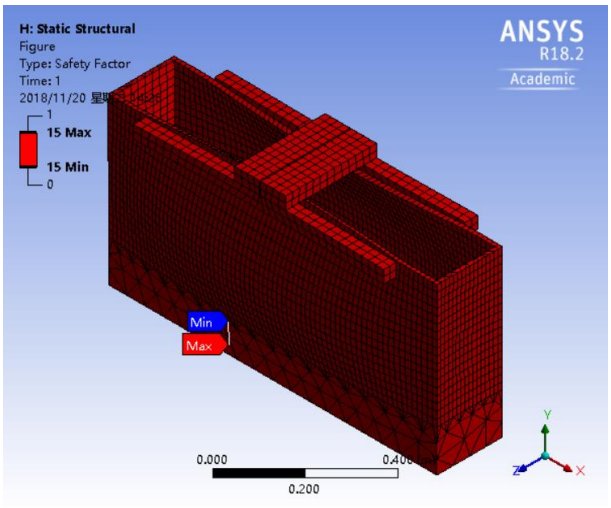

(c)

Figure A.4 Report of Improved Tank When Clamp Is at Center of Long Beams. (a. Total Deformation, b. Equivalent Stress, c. Safety Factor)

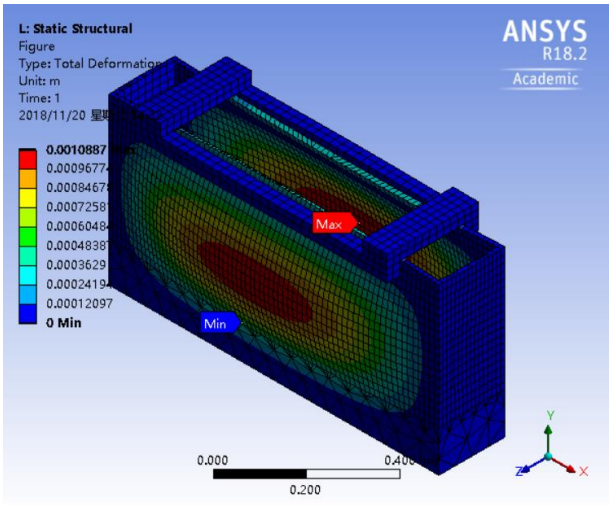

(a)

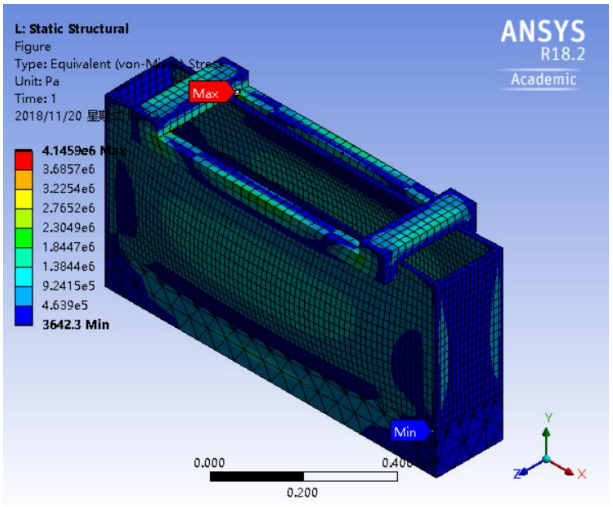

(b)

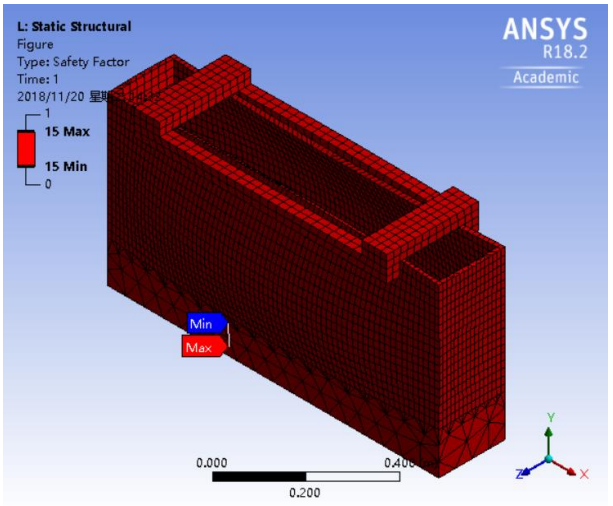

(c)

Figure A.5 Report of Improved Tank When Clamp Is at End of Long Beams. (a. Total Deformation, b. Equivalent Stress, c. Safety Factor)

APPENDIX B: EXPERIMENT DATA OF NEW & OLD GREEN LANTERNS

Table B.1 Brightness at Opening of Green Lantern 2.0 (Unit: lux)

Location	Left Edge	25%	50%	75%	Right Edge
1st Measurement	5450	5900	9610	10530	7430
2nd Measurement	5500	5120	9200	10400	7830
3rd Measurement	5630	5490	9710	10570	7090
Average	5526.67	5503.33	9506.67	10500.00	7450.00
Standard Deviation	92.9157	390.1709	270.2468	88.8819	370.4052

Table B.2 Brightness at Opening of Green Lantern (Unit: lux)

Location	Left Edge	25%	50%	75%	Right Edge
1st Measurement	1880	2630	2540	2570	2340
2nd Measurement	2180	2630	2560	2490	1990
3rd Measurement	2170	2630	2550	2550	1800
Average	2076.67	2630.00	2550.00	2536.67	2043.33
Standard Deviation	170.3917	0.0000	10.0000	41.6333	273.9221

Table B.3 Brightness 50cm away above Opening of Green Lantern 2.0 (Unit: lux)

Location	Left Edge	25%	50%	75%	Right Edge
1st Measurement	3560	4860	6370	6450	5160
2nd Measurement	3310	4700	6160	6020	5460
3rd Measurement	3640	4630	5860	6430	5270
Average	3503.33	4730.00	6130.00	6300.00	5296.67
Standard Deviation	172.1434	117.8983	256.3201	242.6932	151.7674

Table B.4 Brightness 50cm away above Opening of Green Lantern (Unit: lux)

Location	Left Edge	25%	50%	75%	Right Edge
1st Measurement	1370	2190	2320	1200	1290
2nd Measurement	1450	2250	2290	2100	1670
3rd Measurement	1410	2210	2290	2090	1780
Average	1410.00	2216.67	2300.00	1796.67	1580.00
Standard Deviation	40.0000	30.5505	17.3205	516.7527	257.0992

Table B.5 Light Sheet Thickness of Green Lantern at 50cm above Opening (Unit: cm)

Location	Left Edge	25%	50%	75%	Right Edge
1st Measurement	2.0	1.8	1.8	1.8	1.9
2nd Measurement	1.9	1.8	1.9	1.8	1.9
3rd Measurement	1.9	1.8	1.8	1.8	1.9
Average	1.93	1.80	1.82	1.80	1.90
Standard Deviation	0.0577	0.0000	0.0289	0.0000	0.0000

Table B.6 Light Sheet Thickness of Green Lantern 2.0 at 50cm above Opening (Unit: cm)

Location	Left Edge	25%	50%	75%	Right Edge
1st Measurement	1.8	1.9	1.8	1.8	2.0
2nd Measurement	1.9	1.8	1.9	1.9	2.0
3rd Measurement	1.9	1.8	1.7	1.9	1.9
Average	1.87	1.83	1.80	1.87	1.97
Standard Deviation	0.0577	0.0577	0.1000	0.0577	0.0577

Table B.7 Light Sheet Thickness of Green Lantern at Opening (Unit: mm)

Location	Left Edge	25%	50%	75%	Right Edge
1st Measurement	6.0	5.0	5.0	5.0	6.0
2nd Measurement	6.0	5.0	5.1	5.0	6.0
3rd Measurement	6.0	5.0	5.0	5.0	5.5
Average	6.00	5.00	5.03	5.00	5.83
Standard Deviation	0.0000	0.0000	0.0577	0.0000	0.2887

Table B.8 Light Sheet Thickness of Green Lantern 2.0 at Opening (Unit: mm)

Location (mm)	Left Edge	25%	50%	75%	Right Edge
1st Measurement	6.0	5.0	6.0	6.0	6.5
2nd Measurement	6.0	5.0	5.5	5.8	6.5
3rd Measurement	6.0	5.5	6.0	6.0	7.0
Average	6.00	5.17	5.83	5.93	6.67
Standard Deviation	0.0000	0.2887	0.2887	0.1155	0.2887

Table B.9 Temperature Vs Time for Heat Sink of Green Lantern 2.0

Time (min)	0	3	4	5	6	7
Temperature (°C)	20.6	32	34.3	36.4	38.1	39.8
Time (min)	8	9	10	11	12	13
Temperature (°C)	41.2	42.7	44.2	45	46.3	47.3
Time (min)	14	15	16	17	18	19
Temperature (°C)	48.4	49.5	50.3	51.6	52.6	53.4
Time (min)	20	24	29	34	50	62
Temperature (°C)	54.2	57	60.5	63.4	65	70.3
Time (min)	67	71	75	77	83	85
Temperature (°C)	71.8	72.9	73.8	74.1	74.8	75
Time (min)	88	95	100	102	114	120
Temperature (°C)	76	76.4	77.3	77.4	78.9	79

Table B.10 Temperature Vs Time for Heat Sink of Original Green Lantern

Time (min)	0	1	2	3	4	5
Temperature (cm)	21.2	22.5	23.6	25	26	26.6
Time (min)	7	11	15	20	26	29
Temperature (cm)	28	31.5	33.4	35.6	38.1	38.9
Time (min)	32	36	40	43	47	50
Temperature (cm)	39.8	40.8	41.9	42.4	42.9	43.5
Time (min)	57	61	65	70	73	76
Temperature (cm)	44.1	44.6	44.9	45.3	45.4	45.8
Time (min)	81	84	88	93	99	101
Temperature (cm)	45.9	46.1	46.2	46.4	46.4	46.6
Time (min)	104	107	111	114	120	124
Temperature (cm)	46.6	46.8	46.9	46.8	47.3	47.6
Time (min)	128	130	133	142	144	146
Temperature (cm)	47.6	47.8	47.9	48	47.9	48.2
Time (min)	148	150				
Temperature (cm)	48.1	48.1				

APPENDIX C: GREEN LANTERN 2.0 MANUAL

C.1 Material Used for Green Lantern 2.0

Table C.1 Materials of LED Box

Item	Quantity	Purpose
OnlineMetals Aluminum Square Tube 6061-T6-Extruded	1	The main Wall for LED Box
Alexandria Industries MM12200 (Cut into 7.87" long)	6	Heat sink for the LED emitters
Edmund Optics 2.25" x 12.0", 2.0" FL, Cylinder Fresnel Lens	4	Focus lens
McMaster-Carr Mirror (Part Number: 2875K23)	1	Reflect light in the box at both sides
McMaster-Carr 6061 Aluminum (Part Number: 8975K513)	1	Side Wall
McMaster-Carr Marine-Grade Moisture-Resistant HDPE (Part Number: 9785T112)	2	Cover useless light
McMaster-Carr Black Delrin® Acetal Resin Bar (Part Number :8662K41)	2	Hold Fresnel lens
McMaster-Carr Button Head Hex Drive Screw (Part Number: 91255A380)	12	Fix lens holder to the wall of LED box

Table C.1 (Continued)

Item	Quantity	Purpose
McMaster-Carr Black-Oxide Alloy Steel Socket Head Screw (Part Number: 91251A148)	24	Fix heat sink to the wall of LED box
McMaster-Carr Alloy Steel Low-Profile Socket Head Screw	16	Fix LED box to 80/20 4 by 4 bracket at both sides of LED box
McMaster-Carr 18-8 Stainless Steel Hex Nut (Part NumberL 92673A119)	40	Fix LED box to 80/20 4 by 4 bracket and 3 by 3 bracket
McMaster-Carr 18-8 Stainless Steel Hex Drive Flat Head Screw (Part Number: 9210A582)	24	Fix Plastic Sheet to 80/20 bracket
McMaster-Carr 18-8 Stainless Steel Socket Head Screw (Part Number: 92196A113)	8	Fix side wall to LED box
80/20 Inc. Part No. 4415-Black	8	Connect plastic sheet to 80/20 beam
80/20 Inc. Part No. 4376-Black	4	Connect two kinds of 80/20 beams
80/20 Inc. Part No. 4304-Black	4	Connect LED box to 80/20 beam
80/20 Inc. Part No. 1515-ULS (Cut into 15.5" long)	4	The support for plastic sheet

Table C.1 (Continued)

Item	Quantity	Purpose
80/20 Inc. Part No. 1530-ULS (Cut into 13" long)	2	Connect LED box to plastic sheet at both sides
LuxeonStarLEDs Green (530nm) Rebel LED on a SinkPAD-II 10mm Square Base - 163 lm @ 700mA	116	Light source

Table C.2 Materials of Electronic Box

Item	Quantity	Purpose
Arlington Industries EB1212BP-1 Electronic Equipment Enclosure Box with Back plate	1	Enclosure for LED drivers
McMaster-Carr Harsh Environment High-Current Distribution Bar (Part Number: 9290T13)	1	Distribute electric power in the enclosure
McMaster-Carr Cover for Harsh Environment High-Current Distribution Bar (Part Number: 9290T26)	1	Cover for distribution bar
McMaster-Carr Panel-Mount AC/DC Circuit Breaker (Part Number: 3931T5)	1	Circuit Breaker
McMaster-Carr Cover for Push Button Style Panel-Mount AC/DC Circuit Breaker (Part Number: 3931T7)	1	Cover for circuit Breaker
Meanwell LED supply with driver IDLC-45-700	6	Power the LED

C.2 Electronic Box Area Specification

The inside of the electronic box is shown in Figure C.1. There are two levels of LED drivers, each level has three LED drivers. As in Figure C.1, the LED drivers are divided into stacks labeled No.1, No.2 and No.3. The LED supply on the top has a T added at the end of its label. For example, the top LED driver in the area No.1 is called 1T.

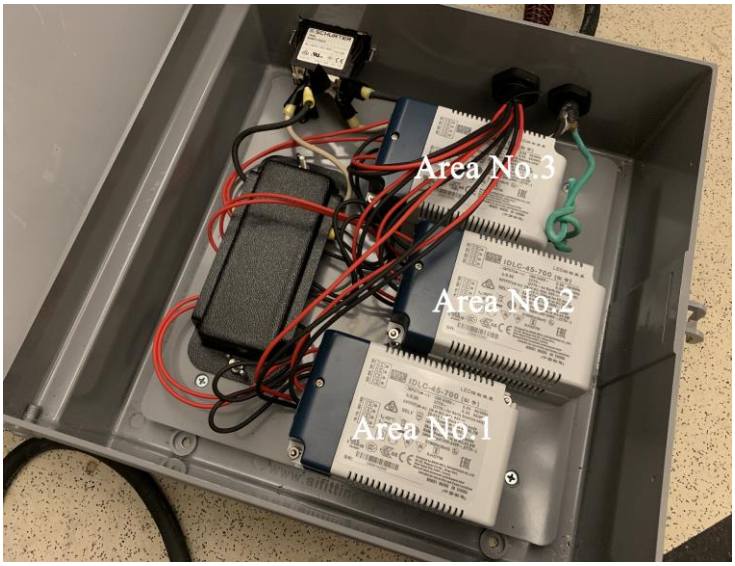

Figure C.1 Electronic Box Configuration

There are labels on the heat sinks from No.1 to No.6 to distinguish the order of the heat sink modules, Figure C.2 and Figure C.3 show the connection orders of the 6-pin connectors at LED box side and electronic box side, of which number 1 to 6 mean the heat sink module number. Figure C.4 shows the connection order between the heat sinks and the LED drivers.

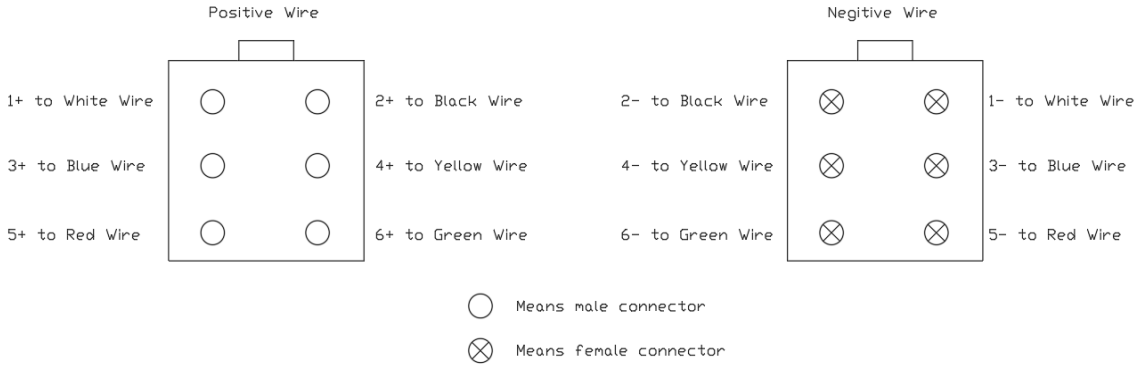

Figure C.2 Connection Order at LED Box Side

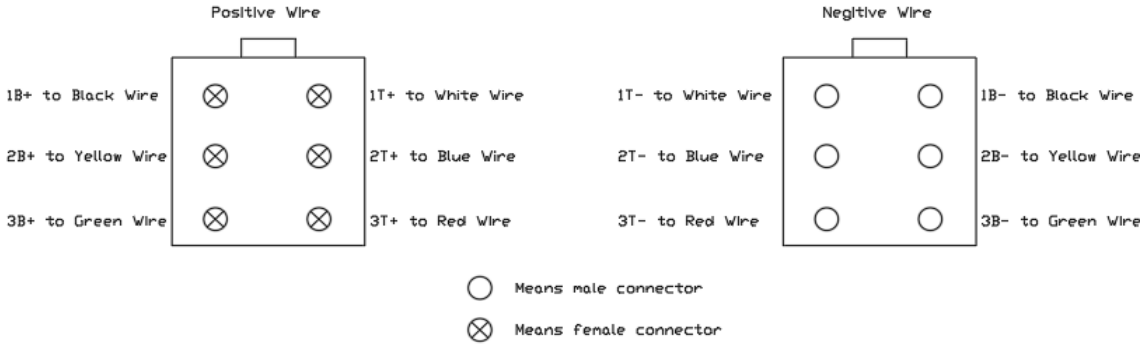

Figure C.3 Connection Order at Electronic Side

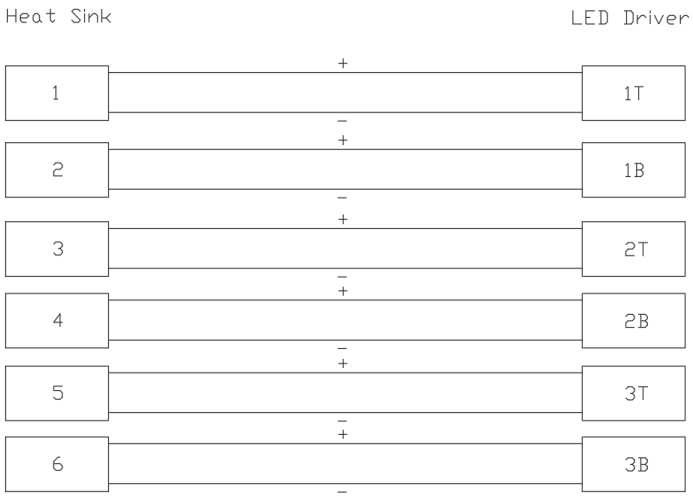

Figure C.4 Connection Order between Heat Sinks and LED Drivers